Deformable Registration of Supine and Prone Colons for CT Colonography

Jung Wook Suh

Dissertation submitted to the Faculty of the
Virginia Polytechnic Institute and State University
In partial fulfillment of the requirements for the degree of

Doctor of Philosophy
in
Computer Engineering
with biomedical option

Christopher L. Wyatt, Ph.D., Chair
A. Lynn Abbott, Ph.D.
Aloysius A. Beex, Ph.D.
Tom Martin, Ph.D.
David Y. Gao, Ph.D.

October 25, 2007
Blacksburg, Virginia

Keywords: Image registration, CT colonography, Virtual colonoscopy

Deformable Registration of Supine and Prone Colons for CT Colonography

Jung Wook Suh

(Abstract)

State-of-the-art three-dimensional endo-luminal virtual colonoscopy (VC) or CT colonography (CTC) is a minimally invasive medical procedure that examines the entire colon in order to detect polyps and colorectal cancer. Most colon cancers malignantly transform from polyps, which are extra growths on the surface of the mucous membrane. Three dimensional endoscopic colon lumen interior images offered by CTC allow physicians to examine the colon interactively. Thus, CTC has several advantages over conventional optical colonoscopy including reduced risk. One of the challenging problems that prevent practical use in clinical situations is the complexity of the human colon. The colon's deformation by peristalsis and the diverse shapes of polyps make it difficult to distinguish polyps from other non-threatening entities in the colon. Hence, most CTC protocols acquire both prone and supine images to improve the visualization of the lumen wall, reduce false positives, and improve sensitivity. Comparisons between the prone and supine images can be facilitated by computerized registration between the scans. In this dissertation, two algorithms for registering colons segmented from prone and supine images are presented. First is an algorithm for three dimensional registration of the prone and supine colon when both are well distended and there is a single connected lumen. Second is another registration algorithm between colons with topological differences caused by inadequate bowel preparation or peristalsis. Such topological changes make deformable registrations of the colons difficult, and at present there are no registration algorithms which can accommodate them. The first algorithm uses feature matching of the colon centerline and a modified version of the demons deformable registration algorithm to define a deformation field between the prone and supine lumen surface. The second method utilizes embedded map representation of colon volume. The two proposed colon registration methods will contribute to improving the accuracy of the computerized registration process and increasing the versatility of the clinical use of CT colonoscopy.

Table of Contents

Table of Figures

List of Tables

List of Abbreviations

CAD	Computer-Aided Diagnosis
CAPD	Computer-Aided Polyp Detection
CT	X-Ray Computed Tomography
CTC	CT Colonography
DFB	Distance From Boundary
DFS	Distance From Source
DRE	Distance between the Radiologist-indicated location and the registration-Estimated location
DRR	Distance between the Radiologist-indicated location and the Rigid transformed location
ITK	National Library of Medicine Insight Segmentation and Registration Toolkit
MR	Magnetic Resonance
MRI	Magnetic Resonance Imaging
OC	Optical Colonoscopy
OR	Overlap Ratio
PDE	Partial Differential Equation
PET	Positron Emission Tomography
SPECT	Single-Photon Emission Coupled Tomography
VC	Virtual Colonoscopy
VTK	Visualization Toolkit
WFUBMC	Wake Forest University Baptist Medical Center
WRAMC	Walter-Reed Army Medical Center

CHAPTER 1. INTRODUCTION AND BACKGROUND

Colorectal cancer is the second leading cause of cancer deaths in the United States. There are approximately 130,000 new cases of colorectal cancer and 60,000 deaths from it each year in the United States [1,2,3]. Most colon cancers malignantly transform from polyps (extra growths from the surface of a mucous membrane). The risk of developing colon cancer can be reduced by early detection and removal of colorectal polyps via screening [17]. CT colonography (CTC) or Virtual colonoscopy (VC) is a minimally invasive technique for examining the whole colon to detect colorectal polyps and colon cancer. Unlike conventional optical colonoscopy, CT colonography is minimally invasive, cost-effective, and largely free of risks and side effects such as perforation and infection. Most of all, CTC is a more patient friendly procedure than conventional optical colonoscopy [17]. Therefore, CT colonography is an advantageous tool for screening and surgical planning.

One of the challenging problems in clinical situations is caused by the complexity of the human colon. Colon deformation by peristalsis and the diverse shapes of polyps make it difficult to distinguish polyps from other non-threatening entities in the colon [22]. The presence of liquid stool also increases the difficulty of examining the colon lumen for detection of polyps. Remaining stool without contrast enhancement will conceal different locations in the lower parts of the interior colon depending on the position of the patients (prone or supine) for CT scanning. Thus, comparison or a registration technique that combines the prone and supine examination results is required to formulate a complete image for computer-aided diagnosis. This is not only a non-rigid registration problem but also a topological problem because there may be missing parts in the images (supine, prone, or both) due to collapsed regions in the colon. These missing parts cause topological differences which renders the conventional registration process infeasible. This problem of topological differences has not been studied because of the high difficulty in reconstructing the missing parts of the colon (position and shape). Also, non-rigid registration techniques are still the subject of ongoing research; there is no dominant algorithm for non-rigid registration.

My dissertation offers colon registration methods which can deal with the severe deformation and topological problems of the colon images for CT colonography. To achieve this goal, the research process is subdivided into the following stages.

1. The centerline of the colon is extracted. It is difficult to describe the comparative

location of a part of the colon except by the colon centerline because of the normal colonic movement like peristalsis and the shape changes of the colon caused by the patient's weight when the patient is in the prone position. The colon centerline is usually used for a brief colon shape representation, a polyp location registration, and a path guiding for virtual camera navigation along the colon lumen. In this dissertation, the extraction of a reliable centerline is implemented using Ming *et al.* [17]'s centerline extraction algorithm.

2. The centerlines of the two colons are analyzed to find the matched region between the supine and prone colons. A centerline piecewise matching algorithm is developed as part of a full registration method for supine and prone CT colonography image data. The motivation for this algorithm is that while the supine and prone CTC images as a whole would not match in shape, certain parts of the images match because of the colon deformation.
3. An extended demons algorithm with level-set representation is presented for an effective 3D registration method. A level-set representation of the object boundary using a distance map is presented as an input to demons registration algorithm [47] for supine and prone image data. From this level-set representation, the demons algorithm can register the 3D volumes with high accuracy even though the two binary objects are very separated and less overlapped.
4. An embedded map representation of the segmented images is proposed for registration of segmented colons from CT colonography images when there is a topological difference between the shapes. This occurs when there is a collapsed segment during shifting of the patient between acquisitions. Deformable registration of images undergoing topological change is a relatively unexplored aspect of registration, but one that is important in real world imaging situations, as the application to CT colonography shows.

This dissertation is organized as follows. The following parts of this chapter discuss the necessary background and provide a literature review related to registration, colon, distance transforms, colonography, centerline generation and level set methods. The next two chapters are independent papers in themselves. Chapter two presents a three-dimensional deformable registration method which can deal with severe deformation of colons. The proposed method is a two-step algorithm to register the segmented prone and supine lumens. First, a feature-based

registration is used to align the lumens approximately about their centerlines, defining an initial non-linear deformation field. Second, this initial estimate of the deformation field is refined using a volume-based deformable registration technique such as the extended demons algorithm. In chapter three, a registration algorithm which can handle topological changes to the prone/spine colon registration problem is presented. The topological difference between the shapes occurs when there is a collapsed segment during shifting of the patient between acquisitions. The algorithm presented in chapter three can accommodate such changes.

1.1 Significance of the research

In this dissertation, colon registration methods which can deal with three dimensional deformation between supine and prone colons are proposed. The significance of this project can be considered from three points of view: Clinical importance, novelty, and the influence on related research fields.

As mentioned earlier, colon cancer is the second leading cause of cancer deaths in the United States, and occurs when polyps present in the colon turn malignant. Therefore, early detection of the polyp is very important in reducing the risk of development of colon cancer. Compared with conventional optical colonoscopy, CT colonoscopy has many advantages. Its main advantages are the ability to observe the whole colon quickly without sedation or risk of perforation [41]. However, CT colonoscopy still has many challenges for the practical use in clinical situations. One of the challenging problems is three dimensional severe deformations between supine and prone colons. The colon shape is diverse, even more so than the human face. Besides, shape changes of colons caused by peristalsis and the scanning posture of a patient are non-rigid and non-linear. Thus, it is not a simple problem to register them. Another problem comes from the topological difference due to the possibility of missing parts in the reconstructed CT images by residual stool or inadequate colonic distention. This topological difference of reconstructed colon volume makes it very difficult to detect the polyp from the fully automated analysis of the colon. Therefore, if a reliable method which can deal with severely deformed colons can be obtained, it will contribute to practical use of CT colonoscopy in clinical situations.

From the viewpoint of maturity of the research, this research project is a sole starting trial for the three dimensional deformable registration between supine and prone colons. No previously published work has dealt with three dimensional deformable registration including the topological difference problem. Only one research group [40], from Stanford University, has attempted to register the supine centerline with the prone centerline. However, their approach is not fully three dimensional. A single paper by a research group [45] in France deals with topologically different

two dimensional brain images. Thus, this research may open the door to the solution for the topological difference problem in registration.

Related computer-aided detection and diagnosis (CAD) fields (such as virtual bronchoscopy, virtual angioscopy, virtual cystoscopy, virtual laryngoscopy, virtual myelography, and others [44]) also deal with long tube-like organs and the images of those organs may have similar challenges to those in CT colonoscopy to different degrees. Therefore, the results in this work will also contribute to the other CAD fields.

1.2 Background

To provide the background for this research, several brief explanations are introduced in the following sections. First are the purpose, classification, and other features of registration. Next, descriptions of colon and colon polyps are introduced. Then the background on CT colonography (as related to this problem) is discussed. The objective of CT colonography, the advantages of CT colonography over the conventional optical colonoscopy, and current limitations of CT colonography are explained. After that, the centerline extraction algorithms are discussed, as the centerline plays an important role in CT colonography. A discussion of distance transforms is included because one of the major centerline extraction algorithms is based on it.

1.2.1 Image registration

Image registration is the process of geometrically aligning two or more images of the same scene. Typically, the source image is aligned to the reference image, also called target image, by spatial transformation. Image registration is often used as a preliminary step before other image processing applications. Medical images generated by different modalities such as MRI and SPECT, require image registration for diagnostic purposes.

For clinical use, the images from PET, SPECT and MR Spectroscopy can support excellent functional information while their descriptive information for anatomical structure is insufficient due to low resolution. In contrast, the images from CT, MRI and Ultrasound have good descriptive information but poor functional information. So the image registration or data fusion between PET/SPECT images and CT/MRI images can combine both anatomical information and functional information.

The brain was the first organ to which image registration was clinically applied. The brain, unlike the heart or the abdomen, is a comparatively rigid body, which does not change its shape or

size over a short period of time. Thus, comparatively simple transformations such as translation and rotation can be applied to brain registration within a single subject. In contrast, the internal organs, which are mainly composed of soft tissues, may change their shape over a short period of time. This type of transformation is called “non-rigid” and is much more difficult than rigid cases because of the substantial anatomical variability across individuals and time [38, 39].

The process of image registration always involves finding transformations that relate spatial information conveyed in one image to that in another or in physical space [5]. In case of registration between supine and prone colon in CT colonography, the voxel order CT-scanned at the patient's prone posture does not conform to the voxel order CT-scanned at the patient's supine posture as shown in Figure 1.1. Therefore, either the supine or prone colon data should be flipped before the registration processing using a known rigid transform.

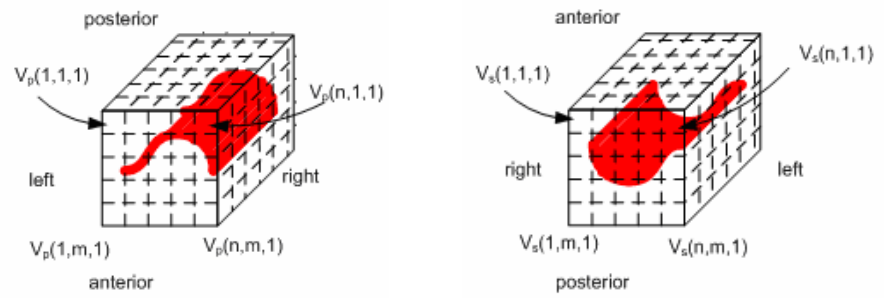

(a) Prone data (b) Supine data

Figure 1.1 CT-scanned data with different order at prone and supine posture.

A deformation vector field is generated after image registration. In case of rigid transforms, the entire deformation field will have uniform vectors, which enable the original shape to be maintained after transform (Figure 1.2 (a)). In case of non-rigid transforms, the deformation vectors vary spatially, however in general, there is a regularization (smoothing) condition required to avoid abrupt change of vectors (Figure 1.2 (b)). Without this smoothing condition, an abrupt change in the vector field makes the registration process unstable (Figure 1.2 (c)).

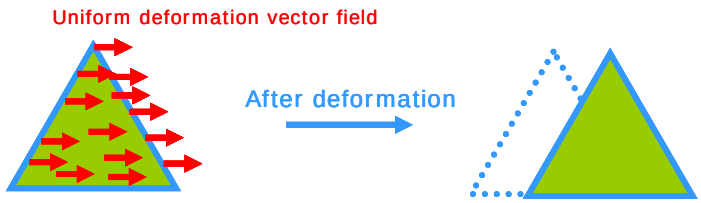

(a) Rigid transform

(b) Non-rigid deformable transform with smooth, regularization condition

(c) Abrupt change of vectors without smooth, regularization condition

Figure 1.2 Effect of deformation vector field

In the demons algorithm, the initial intensity disparity generates the deformation field (Figure 1.3(a)). This initial deformation field is propagated to neighbor pixels by smoothing (Figure 1.3(b)). The deformation process iterates while maintaining local shape structure (Figure 1.3 (c) and (d)). However, when there is no regularization condition, the initial deformation vectors are not propagated to neighboring voxels (Figure 1.4(a)), and the corresponding regions are torn out (Figure 1.4(b)). Therefore, the deformation process becomes unstable and cannot progress. Most non-rigid deformable registration methods have a smoothness constraint in some form. For examples, B-spline terms in spline based non-rigid registrations ([75, 76]) and elastic terms in elastic registration ([77, 78]). In case of topologically different registration, the registration algorithm should allow abrupt change of its deformation field and intensity variation with the

smoothness constraints maintaining stability. This contradiction between stability and representing sharp changes in the deformation field makes registration in the presence of topological differences challenging.

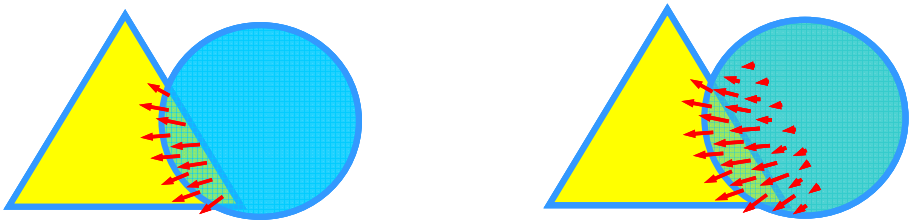

(a) Generation of deformation field by intensity disparities

(b) Propagation of deformation field by smoothing condition

(c) Progress of deformation

(d) Completing step of deformation

Figure 1.3 Example of regularization in demons algorithm

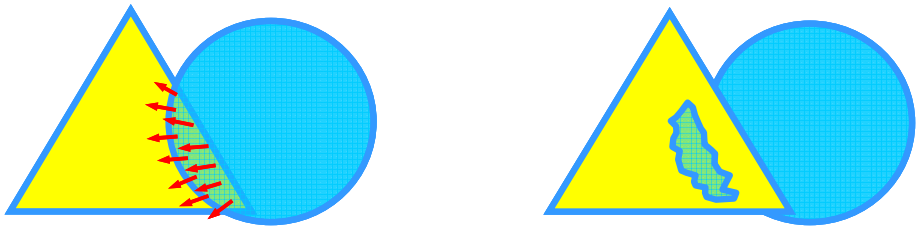

(a) Generation of deformation field by intensity disparities

(b) Some parts are torn out because of no smoothing condition

Figure 1.4 Example of non-regularization case

1.2.2 Colon and colon polyp

The large intestine, also called the colon, extends from the end of the small intestine to the anus. The main role of this long tube-like organ is the water absorption from digested food. The waste products of digestion, called “stool”, are processed in the colon and then excreted through the anus. The stools are moved by “peristalsis” which is a series of wavelike contractions of the smooth muscles in a single direction. The colon is composed of cecum, ascending colon, transverse colon, descending colon, sigmoid, rectum and anus [6] (Figure 1.5).

Polyps are extra growths from the surface of a mucous membrane. These growths range from a millimeter to several centimeters. Flat and broad shaped polyps are called “sessile” and peaked shaped polyps are classified as “pedunculated” (Figure 1.6). Although polyps are not necessarily

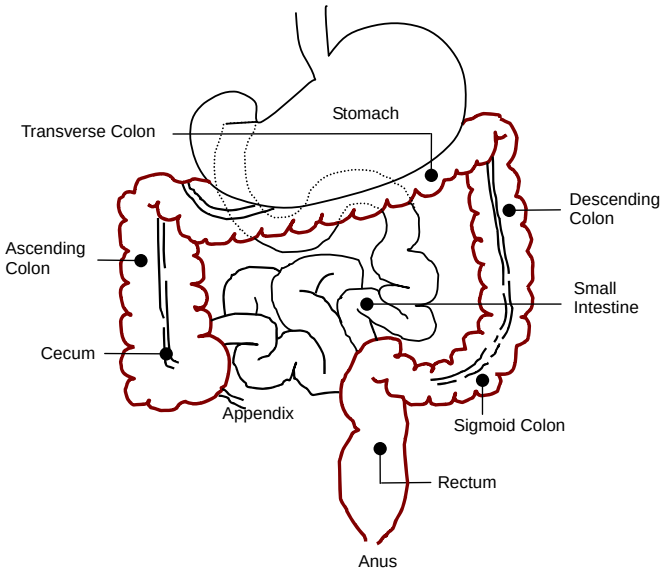

Figure 1.5 Structure of the colon

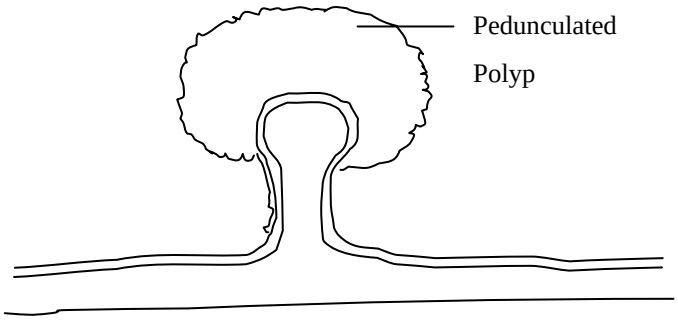

Figure 1.6 Colon polyp

malignant and small colon polyps usually do not present any symptoms, some types of polyps may change into cancer. So gastroenterologists remove all polyps from the patient's body to be safe [7].

1.2.3 CT colonography

CT colonography (CTC) or Virtual colonoscopy (VC) is a minimally invasive technique for examining the whole colon to detect colorectal polyps and colon cancer. Conventional optical colonoscopy uses an endoscope composed of long optical fibers. Optical colonoscopy is invasive and has a risk of perforation (one in 500-1,000 cases)[15]. Sometimes it is not appropriate in examining blocked areas of the colon or in areas of extreme narrowing. In addition, it is uncomfortable from the patients' point of view [16]. In contrast, CT colonography has many advantages, such as being minimally invasive, cost-effective, and largely free of risks and side effects like perforation and infection. Most of all, this procedure is patient friendly: more comfortable and convenient than the conventional optical colonoscopy [17]. According to a recent clinical report [4], CT colonography has the same sensitivity to colorectal lesions 1 cm or larger in diameter as optical colonoscopy. Therefore, CT colonography is an advantageous tool for screening purposes and surgical planning.

The objective of CT colonography is to identify polyps and cancers of the colon. To do this, CT colonography consists of several steps. First, the patient's colon is cleansed and insufflated with CO_2 gas in a similar way to that of optical colonoscopy. In order to obtain a high contrast interface at the colon wall and prevent collapse of the colon, the bulk of feces should be removed through colonic lavage. Gas insufflation makes the colon distended, which provides a high contrast gas/tissue interface. Second, the helical CT scans the patient's abdomen. During 30-45 seconds, helical CT generates 512×512×350 voxels sized 3D volume of body, of which data corresponds to 100~250MB (Figure 1.7). From the CT volume data, colon is segmented and then reconstructed to a graphical 3D volume of the colon (Figure 1.8). Finally, the physician examines the virtual colon to detect possible polyps [18, 19]. Figure 1.9 and Figure 1.10 show the interior of a colon as reconstructed by 3D rendering after segmentation. These kind of interior images offered by CT colonography allow physicians to examine the colon interactively with endoscopic views [20]. In spite of endoscopic views from CT colonography, the complete navigation through the entire colon is not easy for inexperienced physicians because of the possibility of losing track of the position and orientation of the colon. Therefore, the colon centerline is usually used for guiding an automatic or interactive navigation along the colonic lumen. This colon centerline helps to reduce the difficulty and time needed for navigating through the colon [21].

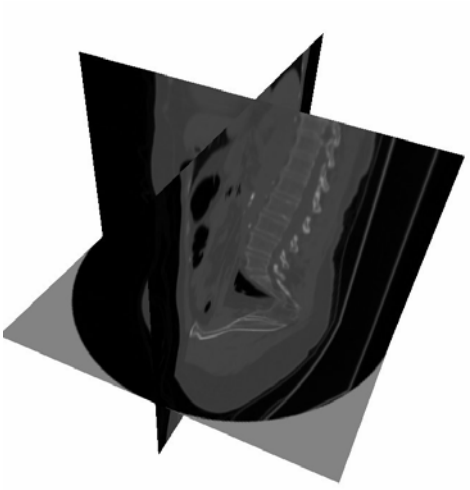

Figure 1.7 Reformatting orthogonal slices for 3D volume from helical CT scans

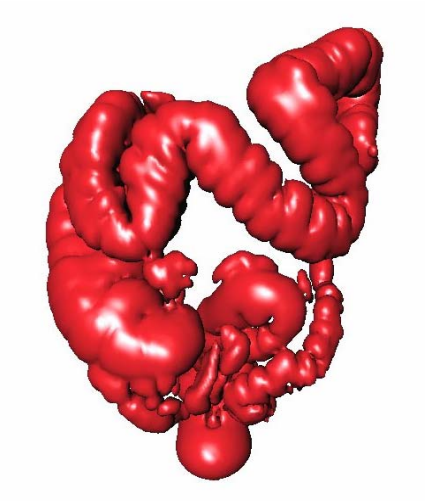

Figure 1.8 Segmented and surface-rendered colon

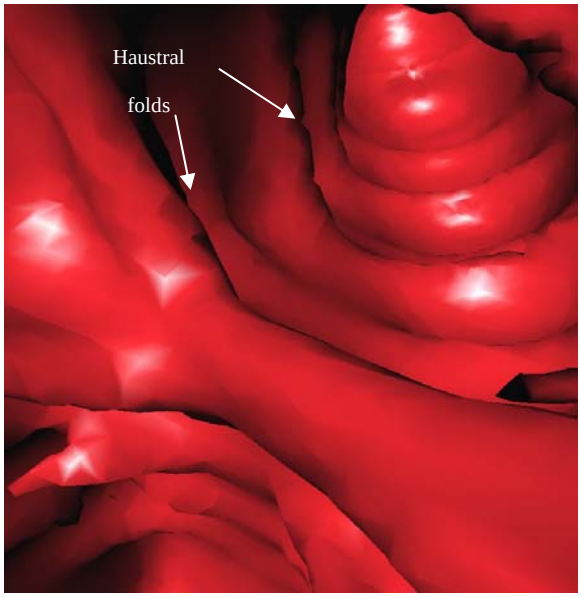

Figure 1.9 Endoscopic view:
Interior of colon with haustral folds

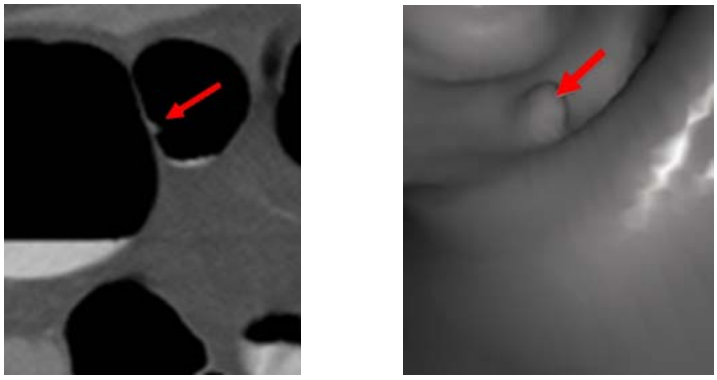

(a) 2D colon from CT scan (b) A polyp in the reconstructed surface

Figure 1.10 Endoscopic view:
A 5 mm polyp within the sigmoid colon

Despite the multiple advantages of CT colonography mentioned above, there are several challenges to its practical use in clinical situations. One of the most challenging problems is the accurate identification of the polyps. Residual feces, the ileocecal valve and thick haustral folds look similar to polyps. In addition, the complexity of the normal colon, its deformation by peristalsis and the diverse shapes of polyps also make it difficult to distinguish exact polyps from the non-threatening entities in the colon [22]. In the case of remaining stool, it is fluid so that it moves along the colon depending on the patient's posture when he or she is scanned by helical CT. Thus, a comparison of the prone and supine examination results is required. Data gathered in the past several years from many patients show that the additional prone scanning with the original supine scanning increases the possibility of detecting polyps [23]. Here is where the registration problem between the supine and the prone images occurs: Registration allows integration of data from prone and supine scans - as opposed to using the data to make individual diagnosis and then integrating the diagnostic results. This is a non-rigid registration process because there are many factors leading to severe deformation of the colon shape between the supine scanning and the prone scanning. The first factor is stool remaining in the colon. This generates the flat air-fluid level depending on the posture of the patient (Figure 1.11). However, the problem caused by the remaining stool can be alleviated by dietary fecal tagging using magnesium citrate and a barium suspension before CT colonography [11]. Another factor for extreme deformation of colon shape is an inadequate colonic distention. The insufflated gas, such as CO_2, for distention is filling the lumen, which provides high contrast gas/tissue interfaces, so the insufficient colonic distention may result in severe topological

deformations of the colon such as collapsed segments of the colon in the reconstructed image (Figure 1.12) while overdistention of the colon can make the thin haustral folds invisible, which also obstruct the registration. As the last factors, the normal colonic movement owing to peristalsis, and the shape changes of the colon caused by a patient's weight when the patient is prone are other main reasons of severe deformation. Although CT colonography has many challenging problems, many studies to overcome those problems and to improve the strong advantages mentioned above are currently in progress.

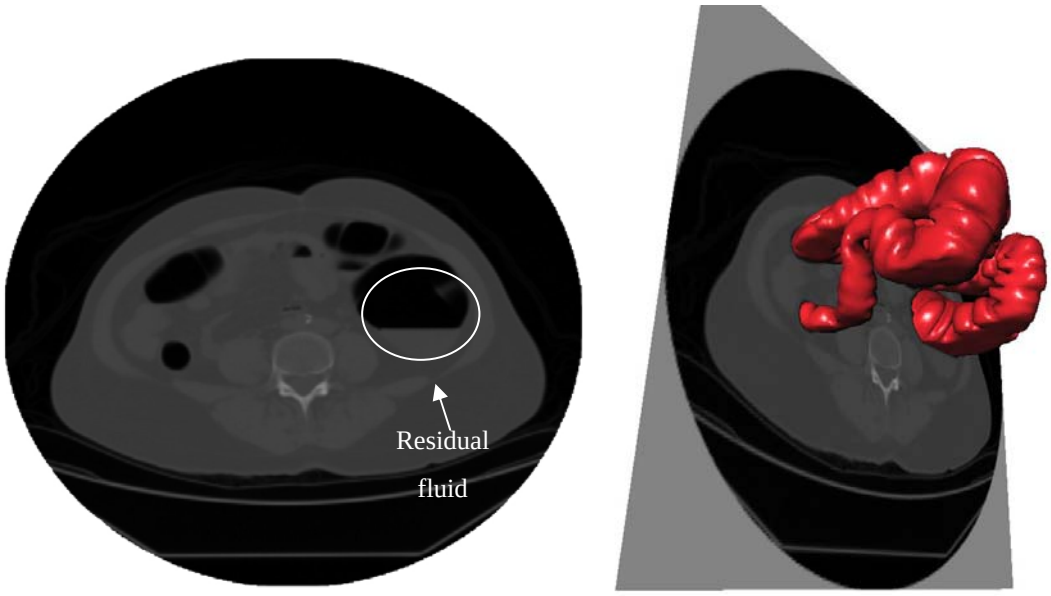

Figure 1.11 Residual fluid in colon (left) and flat rendered surface due to the residual fluid (right)

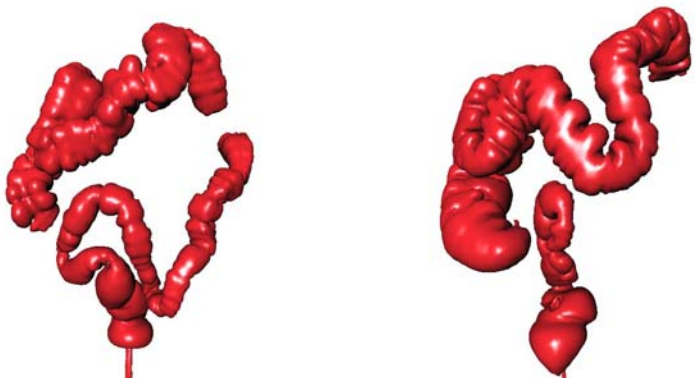

Figure 1.12 Examples of collapsed colon due to inadequate colonic distension and residual stool

1.2.4 Centerline extraction

The concept of centerline, which is also called “medial axis”, “medial path”, or “curve skeleton”, was first proposed by Blum [24]. He defined the centerline as “the locus of centers of maximal disks (in two dimensions) or balls (in three dimensions) contained in the shape” [24]. The general centerlines with many branches may have complicated shapes in normal 3D objects while there is only one centerline after pruning branches in a simple tubular object such as the colon. Because skeletonization, which is the extracte process of the centerline from an object, maintains the generic topology of the object with minimum information on the volume for the original object, the shape representation through the centerline of the object is very useful in many applications such as 3D path planning, character animation, object recognition, shape matching, shape retrieval, and 3D gait analysis [25]. In case of CT colonography mentioned in the earlier section, the centerline for the colon plays important roles including a brief colon shape representation, a polyp location registration, and a path-guiding for virtual camera navigation along the colon lumen. A reliable centerline extraction under a reasonable time limit is still challenging due to the three dimensional complexity of the internal organs, so that many methods have been suggested. These methods can be classified into three categories, depending on their main algorithms: Using topological thinning algorithm, using level set algorithm, and using distance transformation.

Using topological thinning algorithm: This 3D topological thinning algorithm is generally known as the most accurate method for obtaining the skeleton from a 3D object while it requires exhaustive computational power [26]. Thus, most of the centerline extraction algorithms have been suggested as efficient alternatives to the 3D topological thinning algorithm. This algorithm iteratively removes the layers of a 3D object like peeling an onion until there is only one central layer left, which can be regarded as the skeleton of the object. According to Hong, *et al.* [27], the generic topological thinning took several hours to extract the centerline from 512×512×512 sized CTC data. Thus, optimizing efforts for this method were suggested by Bouix [28] and Ge [29]. In Bouix’s paper [28], the thinning process of the object is guided by the medial surface. The feature of the medial surface has the negative average outward flux computed over a very small neighborhood. Thus, the accuracy of the centerline highly depends on the accurate calculation of the object’s medial surface. Besides, this method requires a user-defined threshold value to guarantee the connection of the centerline [25]. Ge [29] made the topological thinning algorithm faster from downsampling colon volumes and removing cavities within the colon region before thinning. From these strategies, he could obtain the topologically thinned centerline of the colon in less than 10 minutes. However, the

object topology may be affected by the removal of cavities, and the accuracy of the centerline from the downsampled volume may not be as good as from the original volume [14].

Using level set algorithm: Hassouna *et al.* [30] proposed a level-set based centerline extraction algorithm. They set a new speed function from which the centerline intersects the propagating front of medial voxels. They distinguished the medial voxels from others by making the medial voxels the peaks of the front having the maximum positive curvatures. Their method has advantages of manual interaction not being necessary for the selection of a seed point of the centerline and it can handle complex structures. Deschamps *et al.* [31] used a front propagation equation for the three dimensional minimal path problem between the two end points as the extraction of the centerline. Through a steepest gradient descent, the minimal path between the two points can be found by descending along the gradient which is orthogonal to the propagating fronts. Their method is fast and generates the centerline well but is limited to one branch at a time.

*Using distance transformatio*n: The centerline extraction using the distance transformation is generally considered to be very fast [17]. This method has two major steps for extracting the centerline. First, the distances between the user-specified source point and each voxel inside the three dimensional object are calculated and stored for the next step. In a second step, the shortest path from a certain starting point to the source point is selected by sliding back the gradient of the result of distance transformation. One of the main differences of these distance transformations [13,14,32,33,34] that use the distance transformation for extracting the centerline is the different discretization method of three dimensional volumetric distances. In other words, the main difference is how they deal with neighbor voxels: Six neighbors shared a side with the center voxel, 12 neighbors shared an edge with the center voxel and eight neighbors shared a corner with the center voxel. These three types of neighbors have different distances (d1, d2 and d3, respectively) from the center voxel. Ge *et al.* [34] used the 3-4-5 Chamfer metric, Chen *et al.* [14] used the 10-14-17 metric and Zhou *et al.* [13] used the 1-2-3 metric in order to approximate the most accurate $1-\sqrt{2}-\sqrt{3}$ Euclidean distance metric as d1-d2-d3 values in three dimensions. One of the disadvantages of the centerline extraction using the distance transformation is that this algorithm has a tendency to hug the corners of winding objects, which results in the centerline being located on the “non” centered position of the object as shown in Figure 1.13 [33]. For enhanced centricity of the centerline, Chen [14] and Bitter [33] used an additional distance between each voxel inside the object and the nearest object boundary. This distance is usually called “DFB-distance”, which

means the distance from boundary. Thus, Bitter [33] combined this DFB-distance with DFS-distance (distance from source point) heuristically. According to his paper [33], this method took about 5 minutes to extract the centerline for 512×512×512 sized colon data.

When we evaluate the centerline extraction algorithms, there are several factors to consider [25]. First is whether this algorithm works fully automatically or not, namely, if this algorithm requires manual interaction to specify the starting point or end point of the centerline. Second is whether this algorithm is sensitive to object boundary complexity or not [13]. Internal organs usually have complicated boundaries like the haustral folds in the colon, so the centerline extraction algorithm should be robust even in the case of the complex object surface. Third, the algorithm should not be computationally expensive. Finally, the extracted centerline should maintain the same topology as that of the original three dimensional volume. In turn, the centerline should be able to represent the shape of the original object, and the accuracy of the representative features of the centerline should not be compromised by computational benefits or other factors.

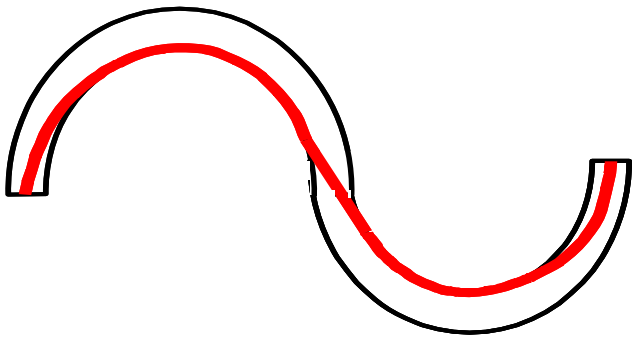

Figure 1.13 Example of “hugging” the corners in the shortest path algorithm

For implementation of colon volume registration, the centerline extraction method of Ming *et al.* [17] was adopted in this dissertation because this method is fast and accurate. Their method is based on the distance transform and makes use of the modified Dijkstra’s shortest path technique to choose the centerline. Although this centerline extraction method was originally designed for guiding a fly-through path for virtual camera navigation along the colon lumen, this method is also expected to be efficient for registration-purposed centerline extraction. Here, I will introduce Ming *et al.*’s centerline extraction method, and then comment on my implementation of their method.

Ming *et al.* used the exact Euclidian distance as the DFB (distance from boundary) distance

and defined the centerline as “the minimum-cost path spanning over the inversed-DFB-distance field inside the colon [17]”. So original volumetric colon data were converted into three dimensional inverse-DFB-distance field. Figure 1.15 shows the process of converting to the inverse-DFB-distance field step by step. From this three dimensional inverse-DFB-distance field, they used modified Dijkstra technique to find the centerline as follows.

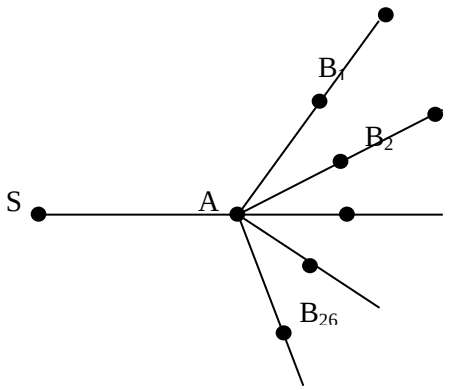

Figure 1.14 Accumulated distance calculation from source via point A

Distance from source point, S, to B_1 ($DFS(B_1)$) is accumulated from $DFS(A) + DIS_{EUC}(A, B_1)$, where $DIS_{EUC}(A, B_1)$ is the Euclidian distance between A and B_1 (Figure 1.14). All of the Euclidian distances ($DIS_{EUC}(A, B_N)$) between A and the unmarked 26 neighbor voxels ($B_1, B_2, \ldots, B_{26}$) around A are calculated, and then their accumulated $DFS(B_1)$, $DFS(B_2)$,….. , $DFS(B_{26})$ are inserted into a sorted heap with their DFB values. This calculation is repeated with the top of the heap as a marked current point until the heap is empty. Here, a heap-sorting algorithm is used to search for the point having the minimum inverse-DFB distance within the heap. Ming *et al.*’s modified Dijkstra algorithm uses a form of the “Greedy Search” algorithm. Unlike the original “Greedy Search” algorithm, this method searches all possible voxels as well as the minimum-cost voxel until the heap is empty. Therefore, this modified Dijkstra algorithm does not fall into the local minimum problem. When I implemented Ming *et al.*’s method, some parts of their method were slightly modified for efficiency. As one can see in Figure 1.16 and Figure 1.17, the integer 3-4-5 distance metric using the three dimensional chamfering mask was adopted instead of the exact Euclidian distance. Consequently, the maximum DFB distance was searched in the heap-sorting algorithm instead of the minimum DFB distance in the original paper. From these modifications, the floating point operations in Ming *et al.*’s method were changed into simple integer additions. Figure 1.18

shows the colon centerlines obtained by this method. The centerlines shown in Figure 1.15 are dilated to the width of three voxels for display purposes; normally they are only one voxel wide.

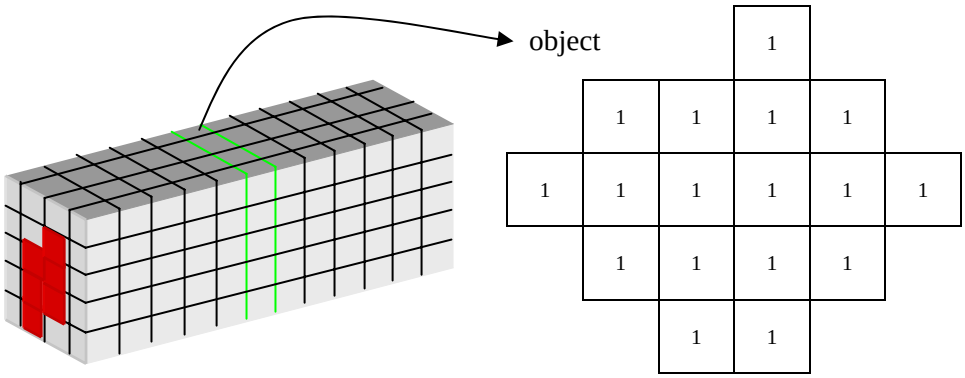

(a) Three dimensional binary volume

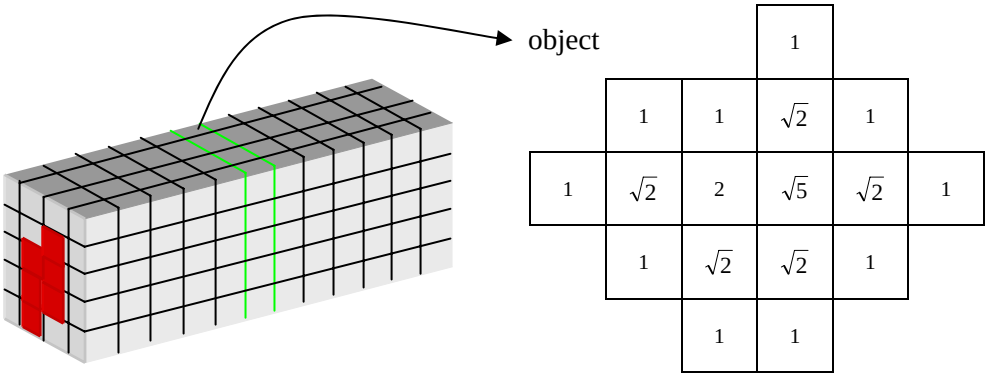

(b) DFB with the exact Euclidian distance

Figure 1.15 The process of the inversed-DFB distance field

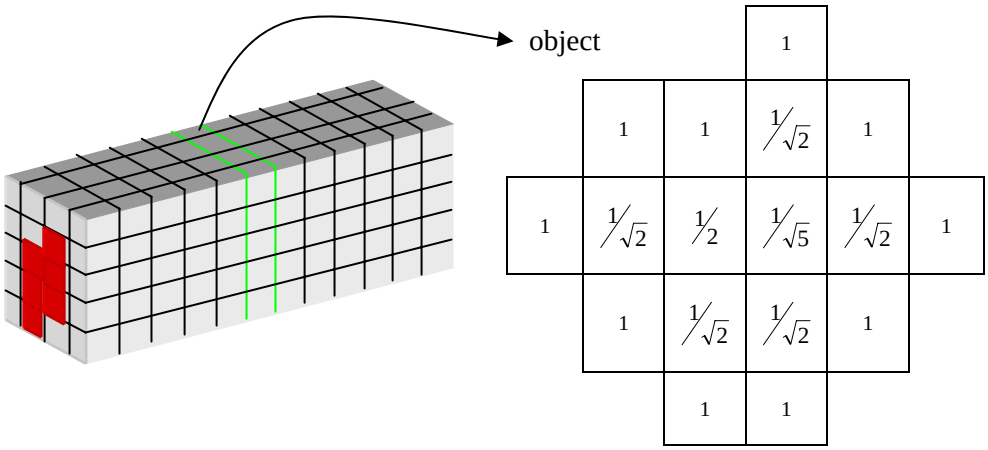

(c) Inversed-DFB distance field

Figure 1.15 The process of the inversed-DFB distance field

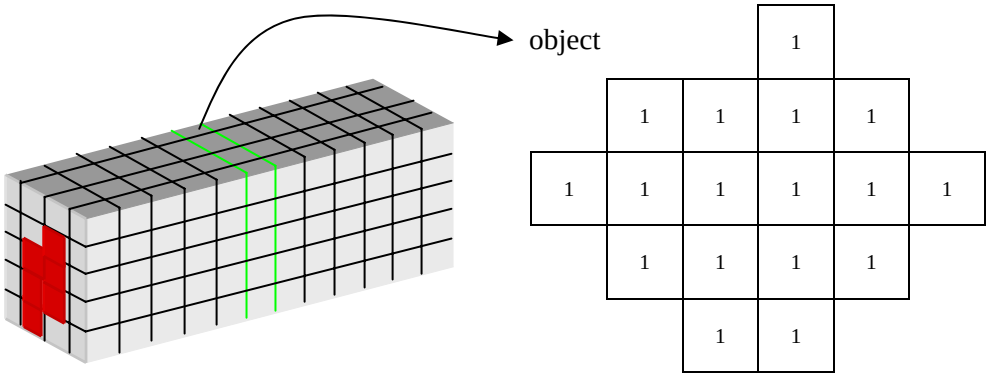

Figure 1.16 The integer 3-4-5 distance metric as DFBs:

Three dimensional binary volume

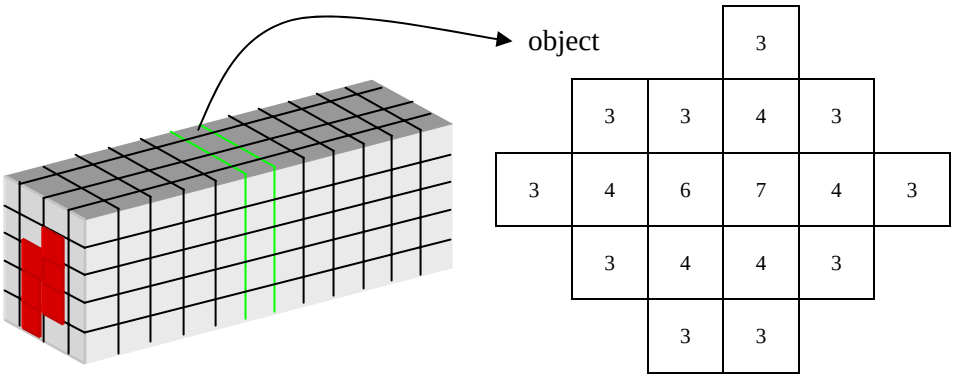

Figure 1.17 The integer 3-4-5 distance metric as DFBs:
DFB through the three dimensional 3-4-5 chamfering

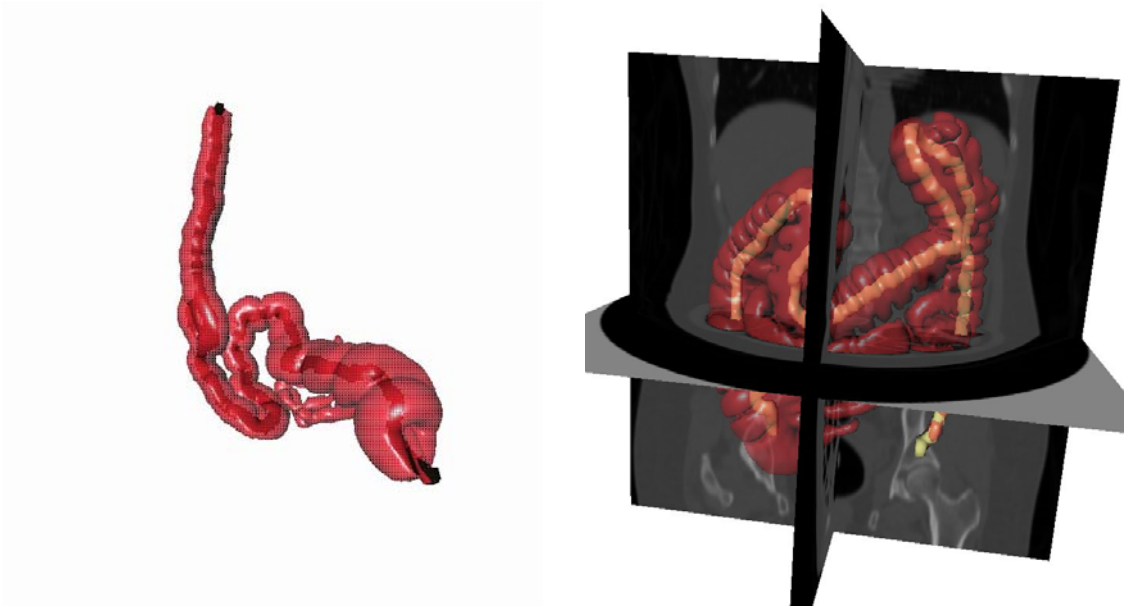

(a) Centerline in a small piece of colon (b) Centerline in a long colon

Figure 1.18 The colon centerlines obtained by modified Ming *et al.*'s method

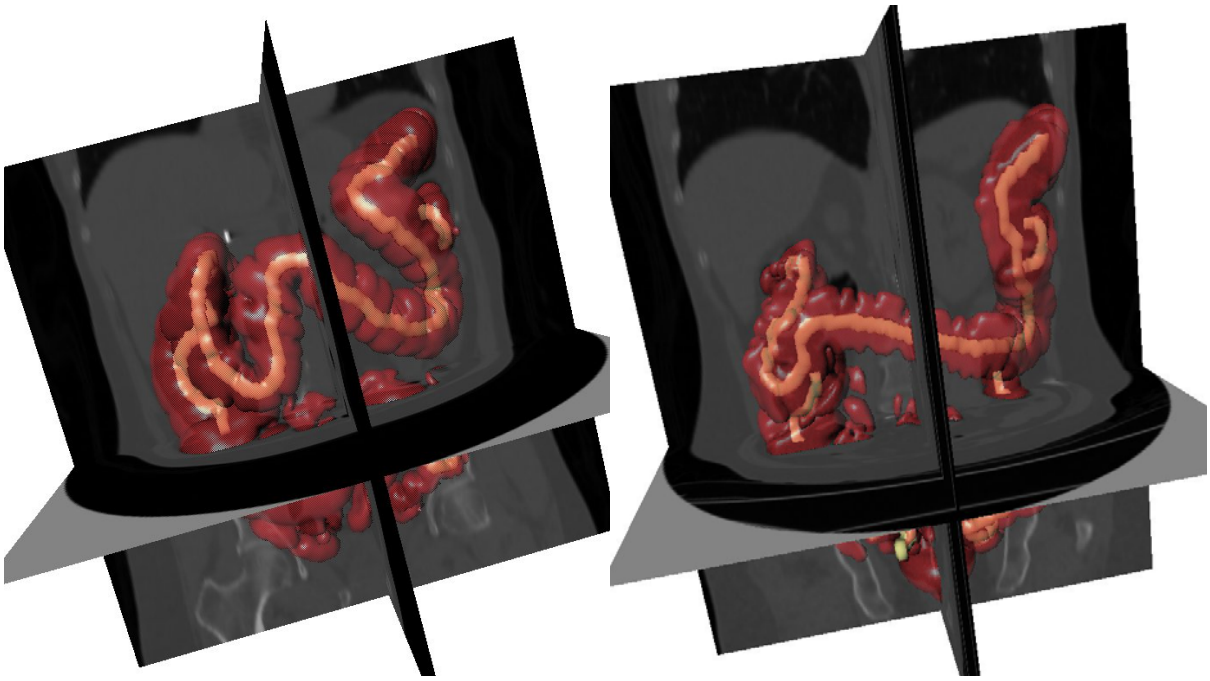

(a) Supine colon and its centerline (b) Prone colon and its centerline

Figure 1.19 Centerline pair of supine and prone colons from a patient.

1.2.5 Distance transformation

The distance transformation generates the distance between one point and an object which is a set of pixels. In order to get the distance from one point to the object, looking up a distance map is much simpler and faster than calculating every distance between one point and all the pixels within the object. This distance map can be obtained by distance transformation from the binary image representing the object. Although the Euclidean distance transformation is exact, the computational burden is relatively high. Therefore, several fast algorithms have been developed to approximate it. Some of these fast algorithms make use of only integer values to calculate the distances, which makes these algorithms more efficient to use in image processing applications [8]. Before considering the several different distance transformations, a "distance metric" should be defined. A distance function $d(p_1, p_2)$ is called a metric if it obeys the following three properties [9]:

1. $d(p_1, p_2) \geq 0$ and $d(p_1, p_2) = 0$ if and only if $p_1 = p_2$: It is always positive or zero.

2. $d(p_1, p_2) = d(p_2, p_1)$: It is symmetric.
3. $d(p_1, p_2) + d(p_2, p_3) \geq d(p_1, p_3)$: It obeys the triangle inequality.

A standard distance metric is Euclidean distance:

$$d_e(p_1, p_2) = \sqrt{(p_{1x} - p_{2x})^2 + (p_{1y} - p_{2y})^2} \qquad (1)$$

Rosenfeld and Pfaltz[3] have shown d_4 and d_8 for the basic city block and chessboard distance.

$$d_4(p_1, p_2) = |p_{1x} - p_{2x}| + |p_{1y} - p_{2y}|$$

$$d_8(p_1, p_2) = \max\{|p_{1x} - p_{2x}|, |p_{1y} - p_{2y}|\} \qquad (2)$$

The d_4 assumes that in going from one point to another one travels directly along pixel grid lines, and diagonal moves are not allowed, while d_8 assumes that a diagonal move counts the same as a horizontal move.

0	0	0
1	0	0
0	0	0

Image

1.0	1.41	2.24
0.0	1.0	2.0
1.0	1.41	2.24

Euclidean distance

1	2	3
0	1	2
1	2	3

d_4

1	1	2
0	1	2
1	1	2

d_8

Figure 1.20 Comparison of three distance metrics

As one can see in Figure 1.20, it is possible to deduce the value of the map in one pixel from the values near it because the distances are not varied abruptly in the distance map. Based on this feature, Borgefors [12] utilized scanning masks to calculate distance transformations efficiently. This method, so called “chamfering” [12], approximates the global distance computation with repeated propagation of local distances within a small neighborhood mask.

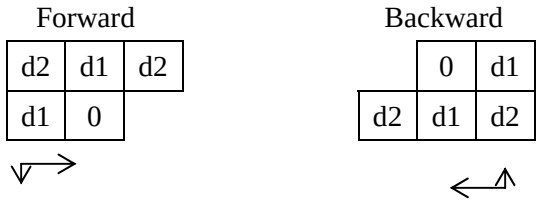

Figure 1.21 Masks for the two-dimensional chamfering

In case of the d_4 metric, d1 = 1 and d2 = ∞, and the d_8 metric has d1 = d2 = 1. The chamfering requires two scans over the image using the masks of Figure 1.21. In the forward scan, the mask starts in the upper left corner of the image, moves from left to right, and from top to bottom. In the backward scan, the mask starts in the lower right corner, moves from right to left, and from bottom to top. The local distances d1 and d2 in the above mask are added to the pixel values in the distance map, and the new value of the zero pixel is the minimum of the five sums [12]. Figure 1.22 shows this process step by step with the d_4 metric:

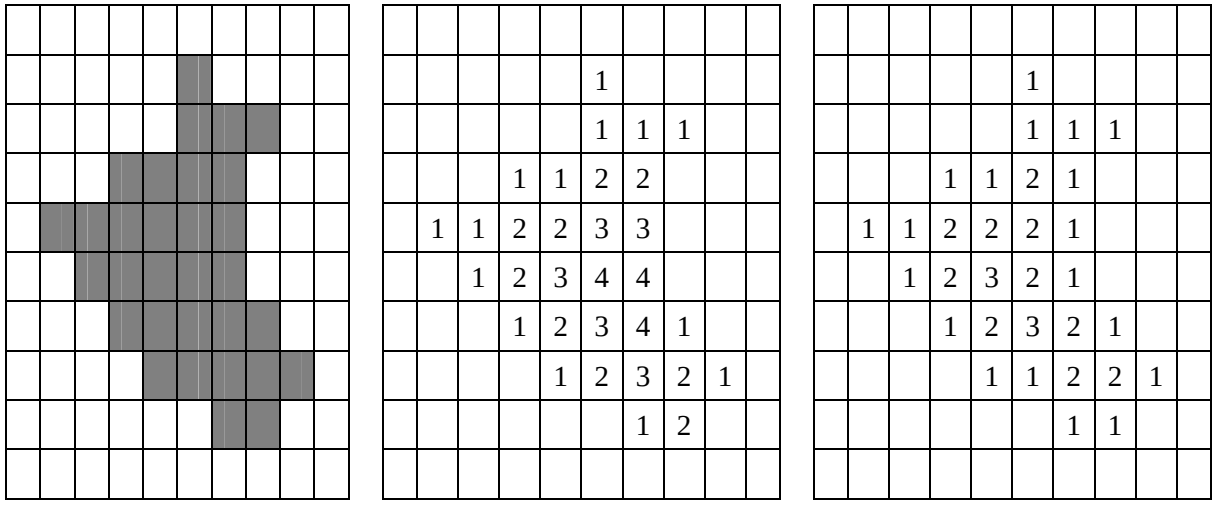

(a) Binary image. Chamfering considers gray pixels as infinities

(b) The result of forward scan with d1 = 1 and d2 = ∞ in the

(c) The result of backward scan with d1 = 1 and d2 = ∞

Figure 1.22 The chamfering result of the d4 distance transformation

In the case of three dimensional volumes, each voxel has 26 neighbors. Six neighbors share a side with the center voxel, 12 neighbors share an edge with the center voxel, and eight neighbors share a corner with the center voxel. These three types of neighbors have different distances (d1, d2 and d3, respectively) from the center voxel. (Figure 1.23)

In order to approximate the most accurate $1-\sqrt{2}-\sqrt{3}$ Euclidean distance metric as d1-d2-d3 values in three dimensions, many metrics including the 1-2-3 metric [13], the 3-4-5 metric [12], and the 10-14-17 metric [14] are suggested and examined (the distance errors decrease in this order as compared with the Euclidean distance). As a compromise between simplicity and distance error, the 3-4-5 metric by Borgefors [12] is widely used as chamfering weights.

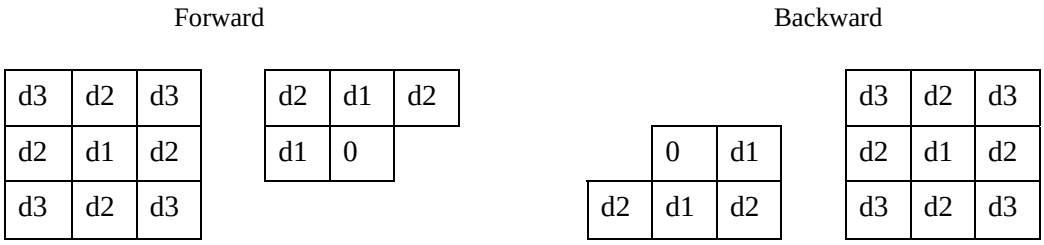

Figure 1.23 Masks for the three-dimensional chamfering

1.2.6 Topology of colon volume

While the term “topology” is a branch of pure mathematics, it can be defined as the description of how spatial features are interconnected [73] or “the continuity of space and spatial properties, such as connectivity, that are unchanged after distortion” [74]. Figure 1.24 shows examples of topologically identical objects and objects with different topologies in 2D.

(a) Topologically same objects

(b) Topologically different objects

(c) Topologically same objects

(d) Topologically different objects

Figure 1.24 Examples of object that are topologically same or different

Figure 1.25 shows an example of topologically different colons. The collapsed region in Figure 1.25 indicates an image disconnection on the CT image (that is distinguished by density differences between air and tissues), not a physical disconnection of the colon. Thus, this collapsed colon image

is a segmentation error caused by inadequate colonic distention or residual stool. Topologically different colon volumes are more frequently observed in CT colonography than single connected colon volumes before fecal tagging.

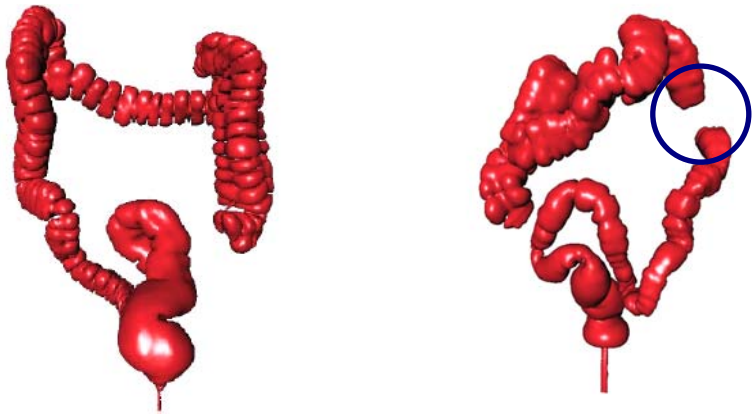

Figure 1.25 Topologically different colon volumes by colon collapse

1.3 Previous work for colon registration

Acar *et al.* [40] proposed registration of the supine and prone colons using the relative colon wall position to the colon centerline. The premise for this approach is that stretching, shrinking and deformation of a colon caused by changing the position of a patient for supine and prone CT colonography can be modeled as piecewise linear mapping functions. Each value of the x, y and z coordinates of the points in the path through the centerline of the colon was used as the inputs to the registration algorithm. As a convention, the +z axis is from feet to head, the +x axis is from the left side of the patient to the right side and the +y axis from posterior to anterior. Authors create piecewise linear functions using the assumption that the beginning and the end points of the prone and supine CT data correspond to the same anatomical points, and morphological similarities exist between the local extrema of the 3D prone and supine CT data along the medial axis colonic path. They make use of the beginning and the end of the transverse colon because these two points are located in the first and second highest positions in +z direction. This algorithm matches each point of the 3D prone and supine CT data recursively for a pre-specified level of recursions or until it cannot find any pair of points that satisfy some criteria. However, there may be more factors causing change in the colon's shape that cannot be described by simple linear stretching and

shrinking with changes in the patient position, although the authors insist that their mathematical functions are enough to describe the changes of the patient position. Their choice of the first and second highest positions in the +z direction as the beginning and the end of the transverse colon may not be applicable to all colons because of the anatomical exceptions. This method does not account for severe deformation of the colon such as colon collapse. Cuzol *et al.* [45] make use of a scalar vorticity of the motion vector field and divergences for source particles in order to model the non-rigid deformation of lesions in multiple sclerosis disease in 2D brain images. However, their 2D non-rigid model does not guarantee performance on the highly deformed cases that have topological differences. As the authors already indicate in their paper: “the extension of their algorithm to the 3D case is challenging because the vorticity is no longer a scalar but a vector. Then a line source or a surface source in the 3D extension should be considered instead of a particle source in the 2D version” [45], the 3D extension requires an excessively long execution time based on complex derivation of the mathematical formulations.

CHAPTER 2. DEFORMABLE REGISTRATION OF SUPINE AND PRONE COLONS FOR CT COLONOGRAPHY

2.1 Abstract

CT colonography (CTC) is a minimally invasive screening technique for colorectal polyps and colon cancer. Most CTC protocols acquire both prone and supine images to improve the visualization of the lumen wall, reduce false positives, and improve sensitivity. Comparisons between the prone and supine images can be facilitated by computerized registration between the scans. In this paper, an algorithm for registering colons segmented from prone and supine images is presented. The algorithm uses feature matching of the colon centerline and a modified version of the demons deformable registration algorithm to define a deformation field between the prone and supine lumen surface. Experimental registration results, when used to determine polyp correspondence between prone and supine images, show an accuracy of 13.77 ± 6.20 mm over 21 datasets with an average Jaccard similarity coefficient of 0.915 ± 0.07.

2.2 Introduction

CT colonography (CTC), also called virtual colonoscopy, produces 3D virtual anatomic models of the colon and is a minimally invasive procedure to detect colorectal polyps and colon cancer [53, 54, 55]. CT colonography has reduced risks of perforation and infection, compared to conventional optical colonoscopy [41] and is currently in clinical trials [56].

CTC requires the radiologist to interrogate a massive amount of CT data to detect polyps. As several studies have indicated, reference information from a computer aided diagnosis (CAD) system can enhance radiologists' diagnostic performance in the detection of polyps [57, 58, 59]. If they can concentrate on regions indicated by CAD, interpretation time can be reduced [60]. For this reason, computer-aided polyp detection will likely be an important part of cost effective CAD in CTC.

Although several variations in scanning protocols exist [61], a typical CTC protocol is as follows. First, the patient's colon is cleansed and insufflated with CO_2 gas in order to obtain a high contrast interface at the colon wall and prevent the colon's collapse. Second, the patient's abdomen

is scanned using helical CT in both the prone and supine position.

The colon is segmented from the CT data and can be rendered to show a graphical 3D representation of the colon (see e.g. [18, 19, 21, 62]). Finally, the physician examines the virtual colon to detect possible polyps, using the original CT images for resolving ambiguities.

The human colon has a complex geometry. Its deformation by peristalsis and the diverse shapes of polyps make it difficult to distinguish polyps from other benign features of the colon [22]. The presence of residual stool, a byproduct of the colon cleansing process, also increases the difficulty in examining the colon lumen for polyp detection. Residual stool may conceal polyps in the anterior or posterior colon when patients are in the prone or supine positions respectively. Various studies [23, 58, 63, 67] have shown the combination of prone and supine scanning increases the sensitivity of polyp detection from 70% (supine only) to 85% (supine and prone) for large ($\geq$1 cm-diameter) polyps and from 75% to 88% for smaller ($\leq$ 0.5 cm-diameter) polyps.

In order to use the prone and supine images in CAD simultaneously we need to register the two lumens. However, there is severe deformation of the colon between the scans. Shape deformations can be caused by the normal colonic movement due to peristalsis and by the patient's weight shifting between positions. In addition, insufficient colonic distention may lead to topological change of the colon shape (collapsed segments).

Acar *et al.* [40] and P. Li *et al.* [46] have developed methods to map candidate polyps between the supine and prone colons using their colon wall positions relative to the colon centerlines. The premise for this approach was that stretching, shrinking and deformation of the colon caused by changing the posture of a patient for supine and prone CT colonography can be modeled by piecewise linear mapping functions. The authors construct piecewise linear functions from the assumption that the morphological similarities existed between the local extrema of the 3D prone and supine CT data along the medial axis colonic path. They determine correspondence of the polyp locations between the supine and prone colons without reconstructing the colon volume because there might be more factors in describing three dimensional change of the colon's shape besides simple linear stretching and shrinking. This estimation of polyp location on the 1-dimensional centerline is not sufficient to incorporate image data including shape and intensity from both scans into CAD directly. Doing so requires a fully deformable registration matching the two lumen surfaces.

In this paper, we present a two-step algorithm to register the segmented prone and supine lumens. First, a feature-based registration is used to align the lumens approximately about their centerlines, defining an initial non-linear deformation field [64]. This step is similar to [40] and [46].

Second, this initial estimate of the deformation field is refined using a volume-based deformable registration technique [51]. We describe a validation study that shows that the combined algorithm can register topologically consistent lumens with Jaccard similarity coefficients of 0.915 ± 0.07 over 21 datasets. The C++ code and example data to reproduce the results are available online at http://www.bsl.ece.vt.edu/ReproducibleResearch/ColonRegistration07/index.html.

2.3 Methods

Figure 2.1 shows the block diagram of the proposed method. First, two centerlines are generated from the segmented source and target volume. Then, either the source or target data is rigidly transformed in order to increase the amount they overlap. In this paper, we rigidly transform the supine colon and its centerline arbitrarily before piecewise centerline matching. Piecewise centerline matching is then carried out using the two centerlines. Based on the difference vectors of the piecewise matched centerline, the difference vectors for other regions are calculated by interpolation and extrapolation. Using the difference vectors for the whole volume, the source data is deformed. This deformed source data and the original target data are used as inputs to the extended demons registration method which matches surfaces precisely.

2.3.1 Feature-based registration by centerline analysis

1) *Centerline Generation:* In order to extract the centerlines from a colon, the centerline extraction method of Ming *et al.* [17] was used. They employed several terms: *DFB* (distance from boundary), *DFS(B)* (distance from source point S to B) and $DIS_E(A, B)$ (Euclidean distance between A and B). Thus, $DFS(B_1)$ is accumulated from $DFS(A) + DIS_E(A, B_1)$ (Figure 2.2). All of the Euclidian distances ($DIS_E(A, B_N)$, $1 \le N \le 26$) between A and the unmarked 26 neighbor voxels ($B_1, B_2, \ldots, B_{26}$) around A are calculated, and then their accumulated $DFS(B_1), DFS(B_2), \ldots$, $DFS(B_{26})$ are inserted into a sorted heap with their DFB values. This calculation is repeated with the top of the heap as a marked current point until the heap is empty. Here, a heap-sorting algorithm is used to search for the point having the minimum inverse-DFB distance within the heap. Ming *et al.*'s modified Dijkstra algorithm uses a form of the Greedy Search algorithm. Unlike the original Greedy Search algorithm, this method searches all possible voxels as well as the minimum-cost voxel until the heap is empty. Therefore, this modified Dijkstra algorithm does not fall into the local minimum problem.

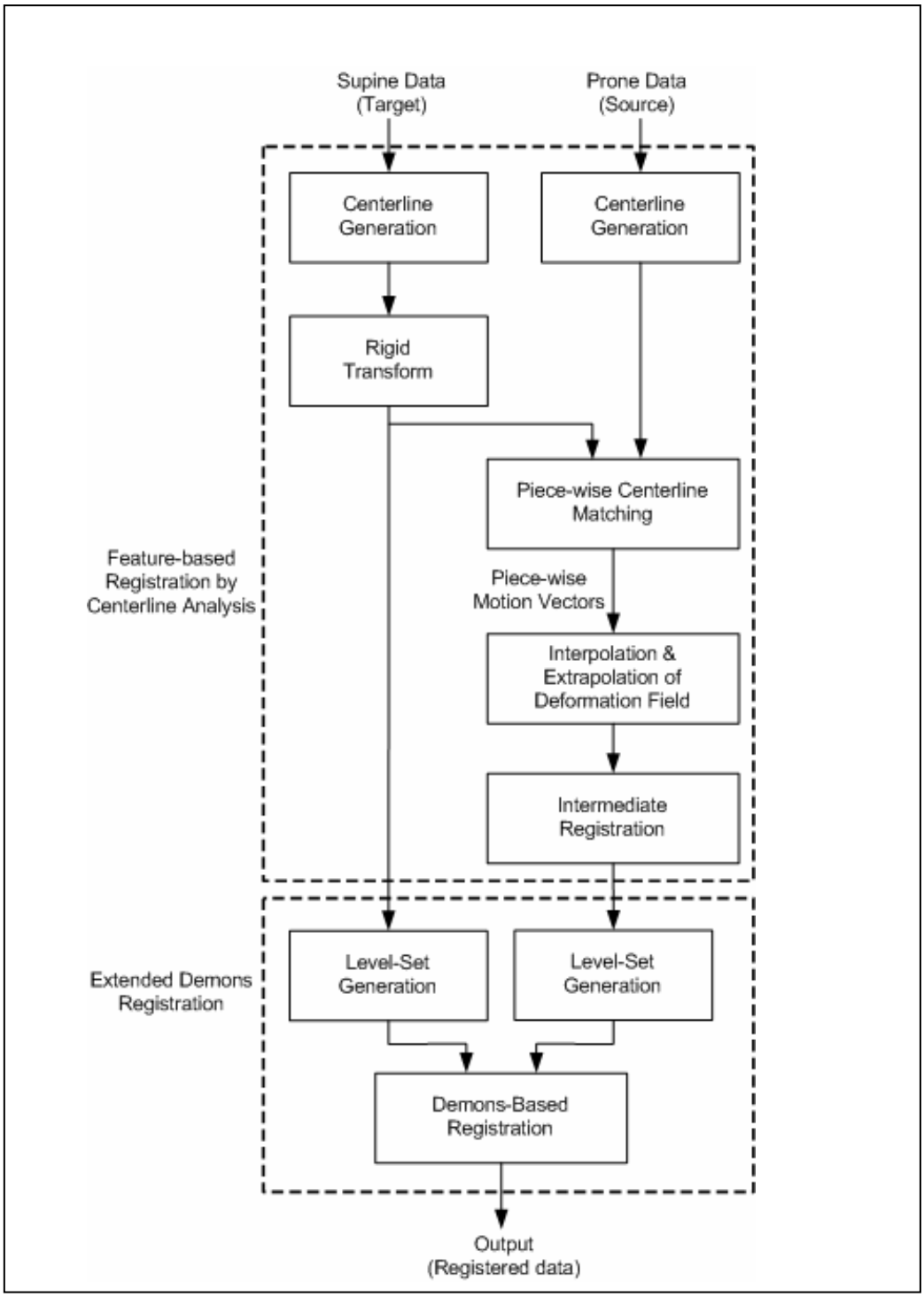

Figure 2.1 Block diagram for the proposed method

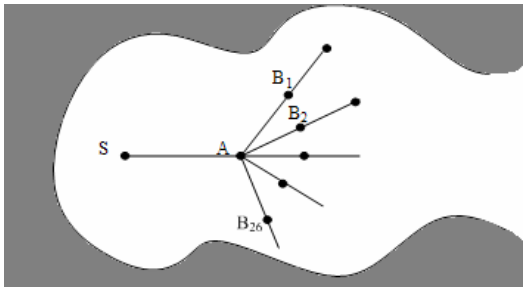

Figure 2.2 Accumulated distance calculation from source point S via point A

2) *Rigid Transform:* This step includes all the rigid transform processes that maximize the overlap ratio (Equation 2 in section 2.3.2.1): First, either the supine or prone colon data must be flipped because the voxel order CT-scanned at the patient's prone posture does not conform to the voxel order CT-scanned at the patient's supine posture. Second, a translation is applied to bring the anus terminal of the centerline into correspondence. The anus is a unique point in relation to the colon that is less influenced by the change in a patient's posture. In the current implementation, the patient's anus point is identified manually by the user. Finally, a rotation about the aligned anus is applied. The axis of rotation and angle is chosen of follows (Figure 2.3). Using the two highest points in z in each supine and prone centerlines, the required rotation angle based on the anus point can be calculated (Figure 2.3 (b)). We simply locate the mid-points of the two highest centerline points in z of the supine and prone colons, respectively. Since the anus points of the supine and prone colon volumes were already aligned in the previous step, the angle required for better overlap of the two volumes was calculated using the three points: the mid-point of the two highest centerline points in supine volume, another mid-point in prone volume and anus point (Figure 2 (b)). Figure 2 (a) shows the two colons before rotation and Figure 2 (c) shows them after rotation. While the overlap ratios (OR) before these alignments (the initial alignment and the rotation) are generally less than 18%, the overlap ratios after these alignments are more than 40%. As we will see in Section 2.3.2.1, the extent of overlap between the source and the target is one of the critical factors which affect the final image registration results. Therefore, this rigid transform plays an important role in the registration accuracy by increasing the overlap ratio between the source and target colons.

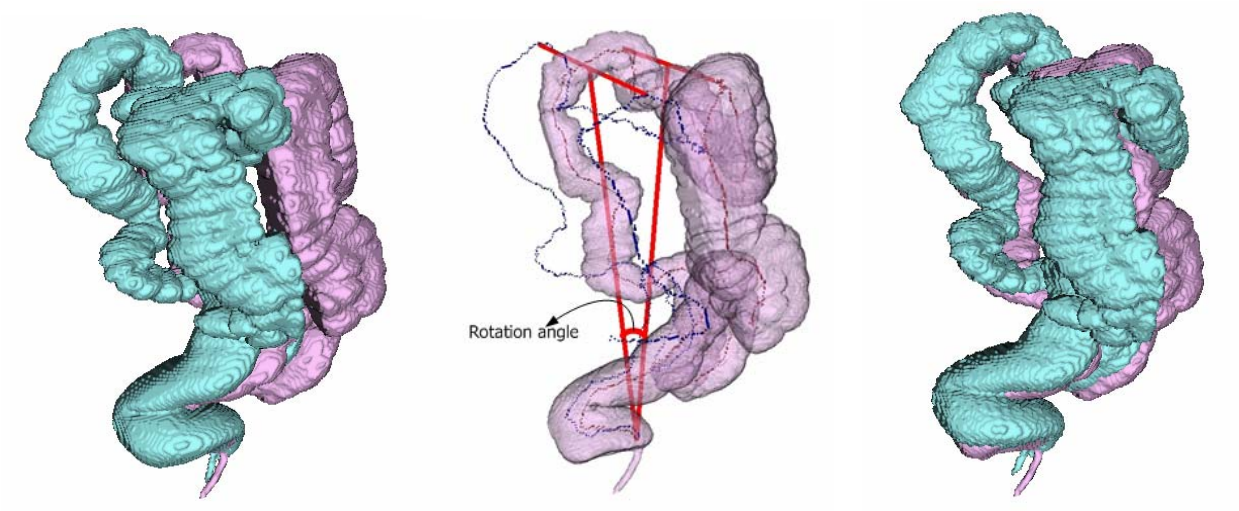

(a) (b) (c)

Figure 2.3 Colon rotation for increasing overlap ratio. (a) Before rotation, (b) Calculation of rotation angle using the two highest centerline points of each prone and supine colon, (c) After rotation depending on the calculated angle in (b).

3) Piecewise Centerline Matching: When the patient's posture is changed for the supine and prone scans, the patient's colon may be deformed and displaced. However, there are still anatomically similar regions in the shape of the colon such as the hepatic flexure, splenic flexure, and sigmoid. These features can be more clearly exposed by the colon centerline. Instead of dealing with each point on the centerline, moving averages of several points on the centerline were used to reduce the trivial effect caused by the point-to-point variation. In Figure 2.4, the horizontal axis represents the moving-averaged centerline voxel indexes from cecum to anus. According to Acar *et al.* [40], the z axis is the most important feature of the centerline. In our case, we used both z and y axes information for the matching of similar centerline pieces. When extrema in z and y axes are found, correlations for the corresponding regions in y and z axes are calculated. For example, if we find a local maximum region in z axis, then we calculate correlation for that region in y axis, and vice versa. When the correlation coefficients for those regions are high, those regions are selected as features on the centerline. In Figure 2.4 (c), the solid vertical bar

and the dotted vertical bar display one of the maximum points in z axis. In Figure 2.4 (b), the solid vertical bar and the dotted bar in y axis display the corresponding point for calculating the correlation. Figure 2.5 shows the centerlines of the supine and prone colons and their piecewise matching results. From these matched points, difference vectors on the featured centerline pieces are computed by simple differences between the two positions.

4) *Deformation Field Propagation:* We adopted the idea from Shen *et al.* [52] of propagating the existing vectors to the neighborhood. Since they used a Gaussian kernel as a propagating method in a different application for different purposes, we used simple linear interpolation and extrapolation. Propagating the difference vectors on the matched centerline pieces is composed of two processes. The first process is the interpolation of difference vectors for the non-matched centerline regions from the matched centerline pieces, and the second is the extrapolation of difference vectors for the whole volume region from the centerline.

a) Interpolation of difference vectors for the non-matched centerline regions: Difference vectors for the non-matched centerline voxels are generated from the difference vectors of the matched centerline pieces. In order to avoid discontinuities at the boundary of centerline points, we used a linear interpolation of the two different difference vectors. Let $\overline{x_1}$ be the position of an end point in the matched centerline piece and $\overline{x_2}$ the position of a starting point in the next matched centerline piece. $V(\overline{x_1})$ and $V(\overline{x_2})$ are their difference vectors. Let $\overline{x_k}$ be a centerline point between $\overline{x_1}$ and $\overline{x_2}$. If $\overline{x_k}$ is a m-th centerline point from the $\overline{x_1}$ and a n-th centerline point from the $\overline{x_2}$ simultaneously, then the difference vector for $\overline{x_k}$ is interpolated as below.

$$V(\overline{x_k}) = \frac{nV(\overline{x_1}) + mV(\overline{x_2})}{m+n} \qquad (1)$$

b) Extrapolation of difference vectors for the whole volume: Since all the centerline voxels have their own difference vectors after completing the interpolation of difference vectors for the non-matched centerline voxels, volume voxels can make use of the difference vector of the nearest centerline voxel. In order to avoid abrupt change of difference vectors of neighboring volume voxels and make the deformation field smooth, the weighted sum of difference vectors from the nearest centerline voxel to the arbitrary 4th nearest centerline voxels (total 9 points) were computed.

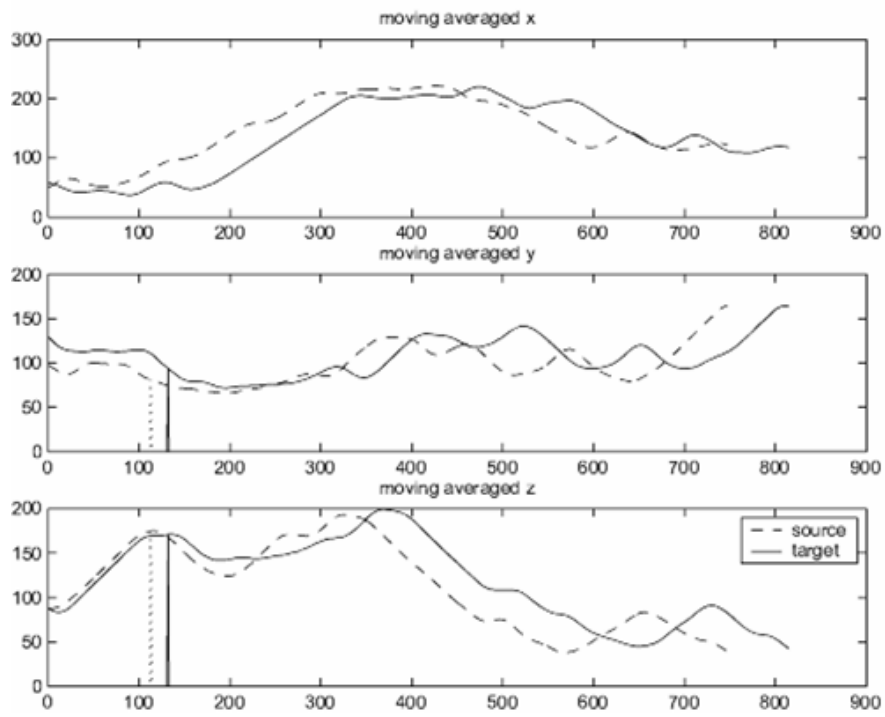

Figure 2.4 Moving-averaged colon centerline in x, y and z direction.

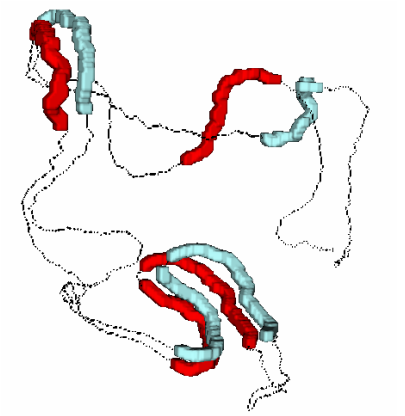

Figure 2.5 Centerlines of the supine and prone colons and their piecewise matching results.

2.3.2 Extended demons registration

As an input to the extended demons registration, we use the source volume previously deformed by the propagated deformation field. For efficiency, the multi-resolution pyramid procedure was adopted in the extended demons algorithm. Four layers were utilized from the coarsest to the finest layer to search the deformation field in this large 3D data set.

1) Demons algorithm: Thirion [47] suggested an image-matching algorithm using a diffusion process. Using the demons concept from Maxwell's demons algorithm in thermodynamics, Thirion considered the non-rigid image matching process as a diffusion process. The theory behind this algorithm is that the object boundary can change its shape depending on the position of the demons within the image domain. The demons' forces, which deform the object shape, are generated to reduce the disparity between the source and the target images. As Thirion indicated in his paper, this algorithm cannot be applied when the two objects do not initially overlap. If the extent of overlap between the source and the target is small, the result of this demons' algorithm does not converge. Therefore, we define the overlap ratio to describe the extent of overlap between the two images as follows.

$$Overlap\ Ratio(OR) = \frac{|S \cap T|}{Area\ of\ \ smaller\ object} \times 100 \qquad (2)$$

Where S is the source and T is the target object. As a similarity measure for shape, we use Jaccard similarity coefficient as below.

$$Jaccard = \frac{|S \cap T|}{|S \cup T|} \qquad (3)$$

Where | S | refers the number of members in the set S as a cardinality.

2) Generation of the level set: For stronger converging performance, we generate the level-set representation [51] of the object boundary using a distance map. There were many attempts to represent a shape using the level-set representation for registration [68,69,70]. We adopt the level-

set representation of the shape for use in Thirion's demons algorithm [47]. Distances inside the object boundary are denoted by negative values, and the distances outside the boundary are denoted by positive values. As figure 2.6 illustrates, this level-set representation allows the demons algorithm to determine the initial demons' force even though the two objects are very separated. Since the segmented colon volume is described only with binary values (the outside is 0 and the inside is 1), the intensity difference between the two objects cannot be accounted for. Thus, the level-set representation of these objects allows the corresponding image region to be maintained as the difference of intensities found in the original demons algorithm implemented in Thirion's paper [47].

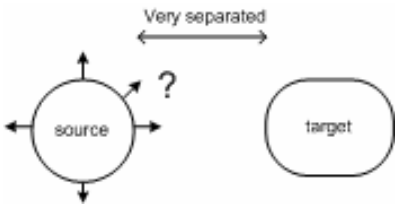

(a)

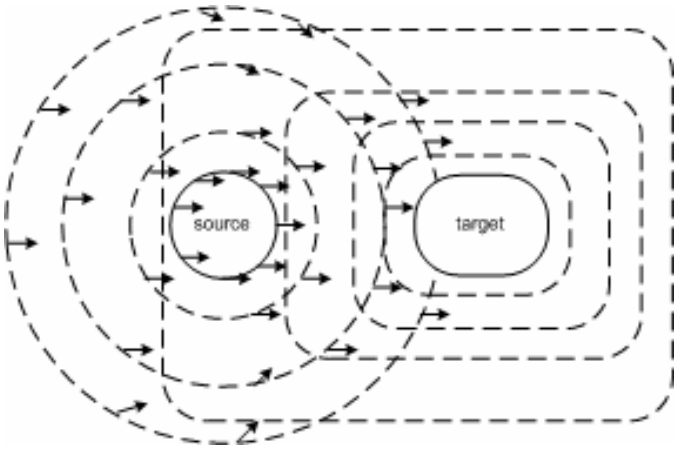

(b)

Figure 2.6 The influence of level sets of very separated objects on Demons' force. (a) Demons' force cannot be decided because of the non-overlapped separation between source and target. (b) Initial direction of Demons' force can be decided by the expanded surfaces of the source and target.

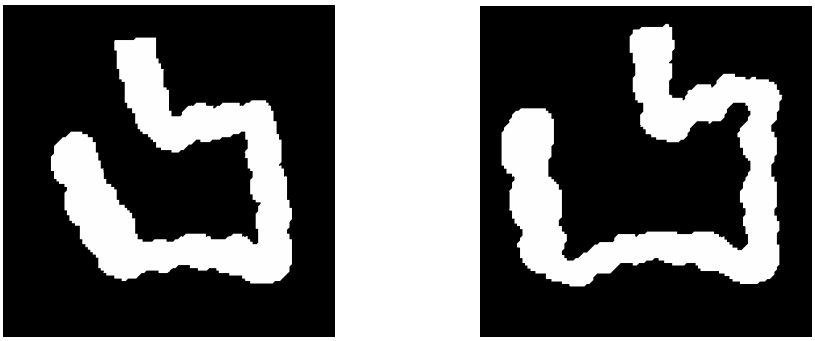

(a) Source image (b) Target image

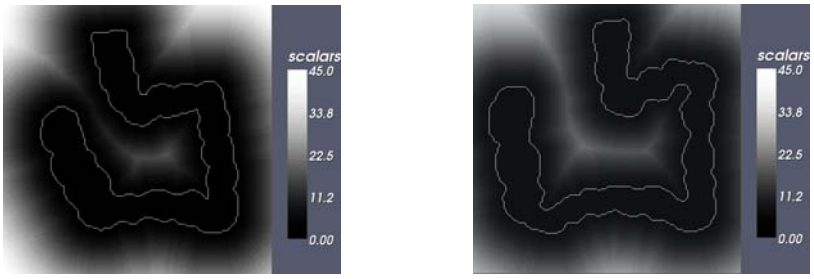

(c) Level set for source image (d) Level set for target image

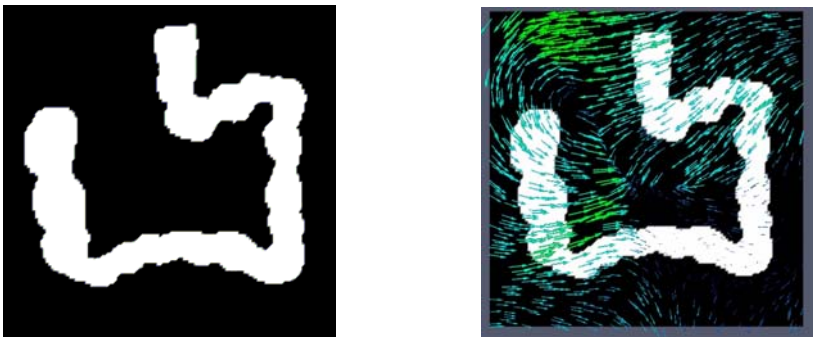

(e) Reconstructed image (f) Deformation field

Figure 2.7 2D example for demons' registration with level set representation.

3) Implementation details: The multi-resolution pyramid procedure was adopted for efficiency. Four layers were utilized from the coarsest to the finest layer to search the deformation field for the large 3D data set. Iteration numbers for each layer were set to 500, 700, 800 and 50 from the finest layer to the coarsest layer respectively. For the implementation of our method, the National Library of Medicine Insight Segmentation and Registration Toolkit [48] (ITK) was used. This open-source

software system was used to support the image segmentation and registration in 2D and 3D data. The Visualization Toolkit [49] (VTK) format was used to store the image data, and ParaView [50] was used to analyze and view the image data. Figure 7 shows the image data after each step in the 2D registration process between the two synthetic images using the extended demons algorithm. Since it is difficult to show the 3D level-set images for the source and the target, the 2D level-set images for synthetic source and target images are shown in Figure 2.7 (c) and (d) for illustration.

2.3 Results

Figure 2.8 shows an example of the simple extended demons registration method. Sometimes the extended demons registration method alone can provide acceptable registration results without feature-based registration (Figure 2.8-c). However, the extended demons registration method has a limitation in that it does not take advantage of any feature information based on the similarity between the two colon volumes. Thus, the registration results may not be satisfactory when one or both of the supine and prone colon volumes have complicated, twisted regions. Figure 2.9 illustrates a case where the extended demons registration method alone generates incorrect correspondence using a hypothetical example. These errors are caused by the extended demons registration method only using distances from the colon wall as a matching criterion.

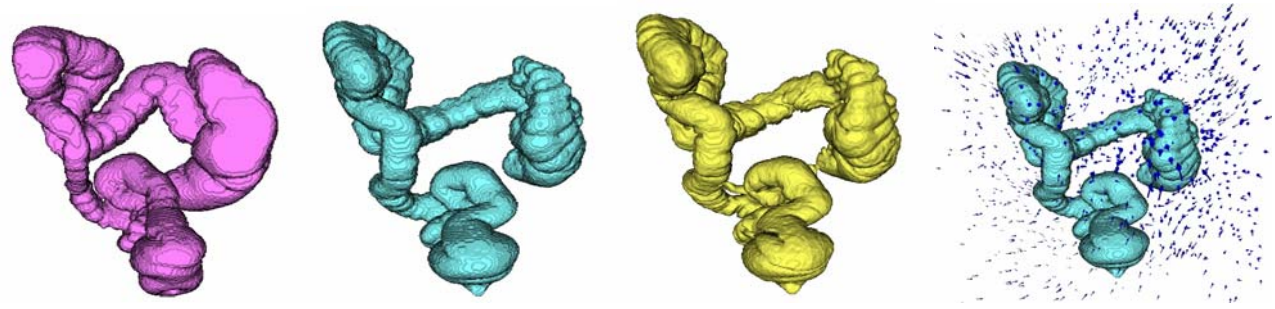

(a) (b) (c) (d)

Figure 2.8 3D example for demons' registration with level set representation. (a) Source supine colon, (b) Target prone colon, (c) Registered colon reconstructed from source supine colon (a), (d) Deformation field generated by the extended demons algorithm alone.

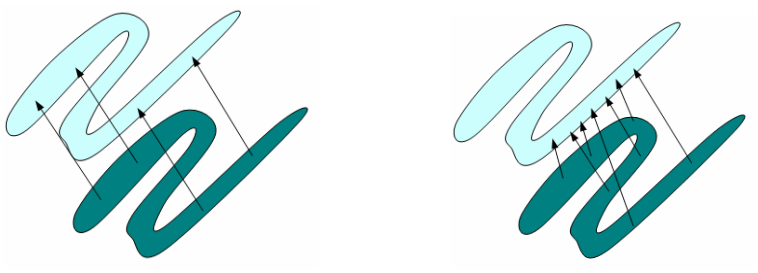

(a) (b)

Figure 2.9 Complicated registration by the demons algorithm (a) Expected correct motion vectors, (b) Incorrect motion vectors by the extended demons algorithm

Therefore, a pre-registration step that matches similar regions in source and target volume is required for the extended demons registration method to produce acceptable results in cases of severe deformation between scans. The feature-based registration by centerline analysis plays the role of a pre-registration step for matching similar regions between source and target volumes.

Figure 2.10 shows the results of the simple extended demons registration method and the proposed method which adds the feature matching information to the extended demons registration method. This experiment was performed on an AMD dual core 1.8GHz processor with 4GB memory for the subsampled CT data (256x256x170). As one can see in Figure 2.10 (d), the reconstructed volume from the simple extended demons method has a crushed region because the corresponding region in the target volume has a complicated shape. However, the corresponding region within the result from the proposed method was accurately reconstructed (Figure 2.10 (e)). It took 17 minutes for both the piecewise centerline matching block and the interpolation & extrapolation of deformation field block in Figure 2.1. Another two and half hours were needed for the extended demons registration block using multi-resolution pyramid procedure (50, 50, 50 and 30 iterations from the coarsest layer to the finest layer, respectively).

We picked five arbitrary points (black dots in Figure 2.10 (a)) from the various regions of the source colon for illustration purposes. After application of the deformation field to these source points, the corresponding five points (black dots in Figure 2.10 (e)) are located near the original points in the source. Through tracking these points, we can ensure the registered volume is not arbitrarily reconstructed so that the result makes sense anatomically. Figure 2.11 shows how the Jaccard similarity varies after each step.

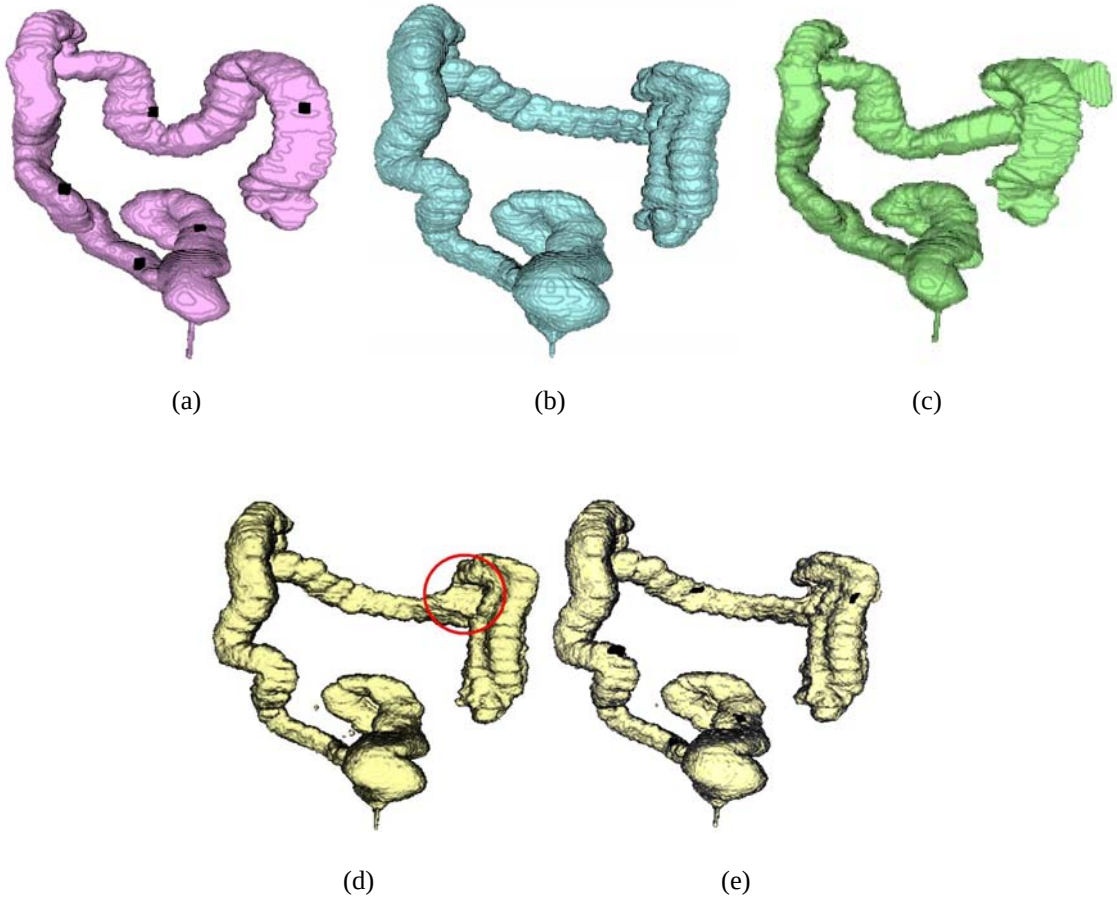

Figure 2.10 Comparison between the result of the simple extended demons method and the extended demons method with piece-wise feature matching. (a) Source colon, (b) Target colon, (c) Intermediate colon by the feature-based registration (d) Result of the simple extended demons method without feature-based registration and (e) Result of the extended demons method with feature-based registration. The black dots in a) and d) are an arbitrary set of corresponding points.

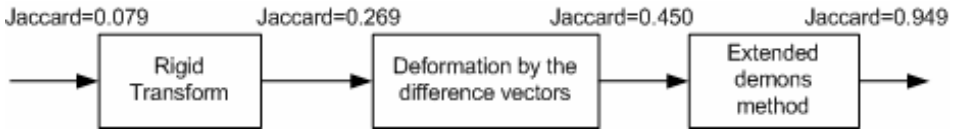

Figure 2.11 Example of how the Jaccard similarity coefficient varies at each step (data same as in Figure 2.10).

.

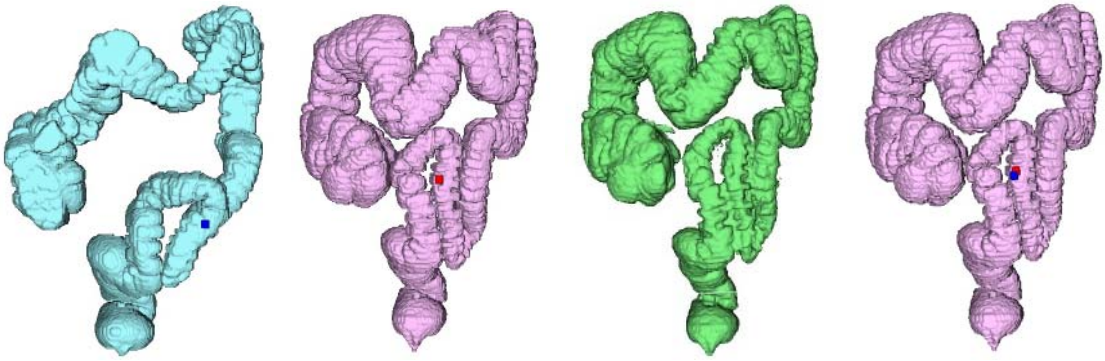

(a) (b) (c) (d)

Figure 2.12. Another patient's colons (with one polyp) and their registration results, (a) Source prone colon, (b) Target supine colon, (c) Registered colon from source, and (d) Comparison of polyp location between the real polyp location (red) at supine colon and the calculated polyp location (blue) from the prone polyp location by the proposed registration method.

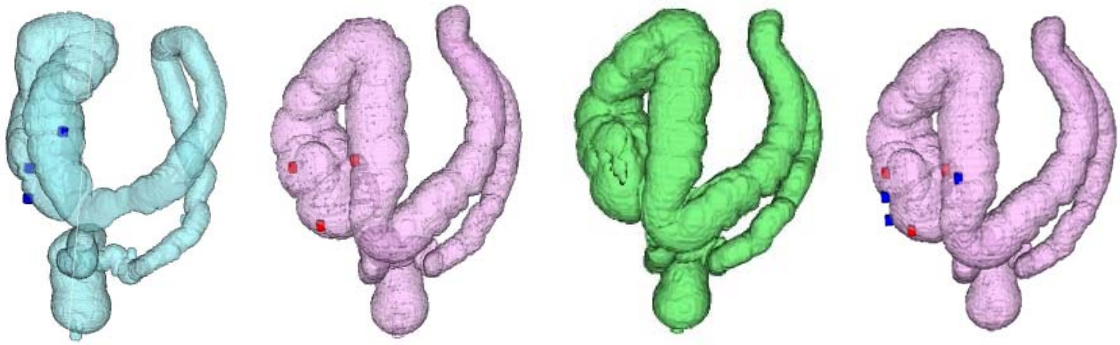

(a) (b) (c) (d)

Figure 2.13 Another patient's colons (with multiple polyps) and their registration results, (a) Source prone colon, (b) Target supine colon, (c) Registered colon from source, and (d) Comparison of polyp location between the real polyp location (red) at supine colon and the calculated polyp location (blue) from the prone polyp location by the proposed registration method.

Using the proposed method, we've obtained a Jaccard similarity coefficient as higher 0.949 (For reference, the Jaccard similarity coefficient of the reconstructed result from the simple extended demons method without the feature matching information was 0.868.). We have 21 experimental data sets from 21 different patients' colons. The final Jaccard similarity coefficients for those 21 are 0.915 ± 0.07. As far as we know, there is no previous work that non-rigidly registers and reconstructs the 3D colon volume. Therefore, no experimental comparison to other methods could be made. We also tested the change of polyp locations between patients' supine and prone data. We used 21 data sets in which polyps were diagnosed by a board certified radiologist.

Table 1. Comparison between the estimated polyps by only rigid transform and by the proposed method (unit: mm)

	Polyp location in supine colon (polyp position in colon)	Estimated polyp location for supine colon by only rigid transform from the polyp of prone colon	Dist.	Estimated polyp location for supine colon by registration from the polyp of prone colon	Dist.
Figure 2.12	(74.0, -132.0, -279.0) (Sigmoid colon)	(137.6, -92.95, -315.84)	83.23	(72.35, -136.45, -289.84)	11.83
Figure 2.13	(-49.32, -112.72, -269.83) (Transverse colon)	(-113.09, -109.21, -244.83)	68.59	(-36.91, -130.74, -274.83)	22.44
	(-107.45, -80.6, -270.83) (Cecum)	(-114.75, -51.24, -274.83)	30.52	(-109.78, -83.99, -287.83)	17.49
	(-84.76, -92.83 -331.83) (Cecum)	(-118.06, -51.23, -306.83)	58.86	(-104.13, -70.14, -326.83)	30.24

Table 2. Result comparison of CT data with different settings

	WFUBMC 6 datasets (5 mm collimation)	WRAMC 15 datasets (2.5 mm collimation)	Total (21 datasets)
Jaccard Similarity Coefficient	0.886 ± 0.11	0.927 ± 0.04	0.915 ± 0.07
Polyp location error by only rigid transform (mm)	44.91 ± 24.81	26.86 ± 14.98	32.02 ± 19.51
Polyp location error by proposed method (mm)	13.81 ± 5.95	13.75 ± 6.50	13.77 ± 6.20

From among those 21 tests, Figure 2.12 and Figure 2.13 show two examples of the patients' colons; their volume registration result, and their polyp location change due to the proposed registration method. In Figure 2.13, we show an example where there are three polyps with polyp registration errors of 17.49 mm, 22.44 mm and 30.24 mm for each polyp respectively. The results are summarized in Table 1 for the two examples.

The rigid transform in Table 1 included the three processes (1. Flipping, 2. Initial alignment based on patient's anus, 3. Rotation) as explained in Section 2.3.1.2. As one can see in Table 1, all polyp locations estimated from the prone polyp location by our registration method are much closer to the supine polyps (as indicated by radiologists) than those using the simple rigid transform. All polyp locations estimated by the proposed method are accurate so that the differences between the radiologist-indicated locations and the registration-estimated locations are 13.77 ± 6.20mm over 21 datasets while the differences between the radiologist-indicated locations and the only rigid transformed locations (without feature matching) are 32.02 ± 19.51mm. Among the 21 colon datasets, 15 datasets are from the Virtual Colonoscopy Resource Center [71], which were acquired with a 2.5 mm collimation at 100 mAs and 120 kVp [72]. The other 6 datasets are from the Wake Forest University School of Medicine and were acquired with a 5 mm collimation at 120 kVp and 180 mAs for the supine position, and at 120 kVp and 80 mAs for the prone position. Table 2 presents the registration accuracy results by acquisition protocol and in total.

In order to statistically verify that the results of the proposed method on polyp location estimation are significantly different from the results of a simple rigid transform, a statistical test was performed. Generally, a p-value from a Kolmogorov-Smirnov test (non-parametric test) close to zero indicates that the null hypothesis is false, which means that a difference between the two collected data is very likely to exist. The calculated p-value for our experiment is 0.001. Because a p-value of 0.01 is a typical threshold to evaluate the null hypothesis in medical applications, it is statistically confirmed that the results of our proposed method are improved over those of the rigid transform only.

2.4 Discussion

In the results of the polyp location estimation, the accuracy was improved by 57.0 % because the averaged DRE (Distance between the radiologist-indicated location and the registration -

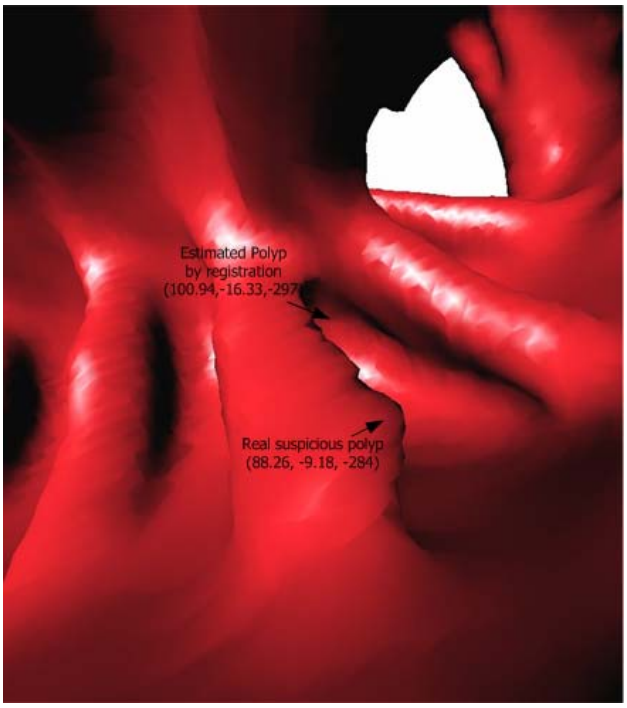

(a)

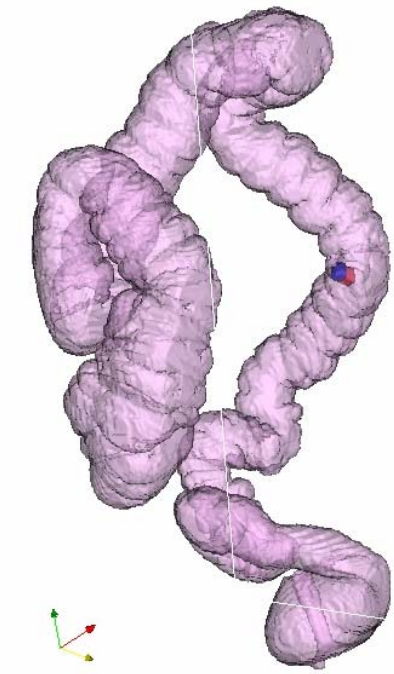

(b)

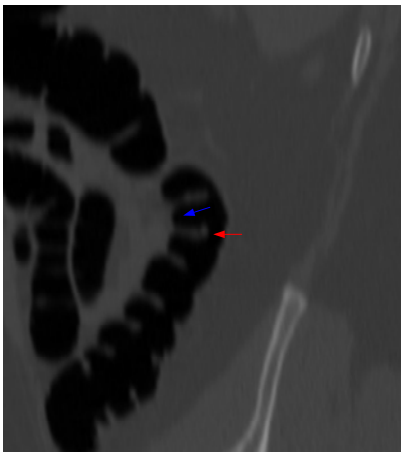

(c)

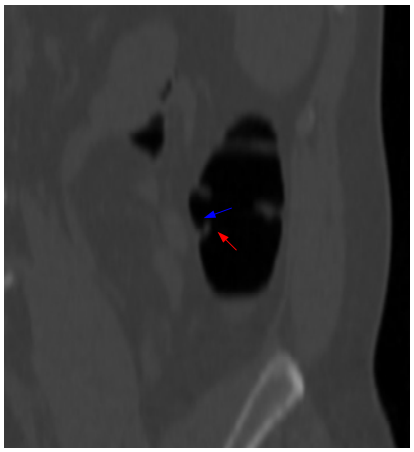

(d)

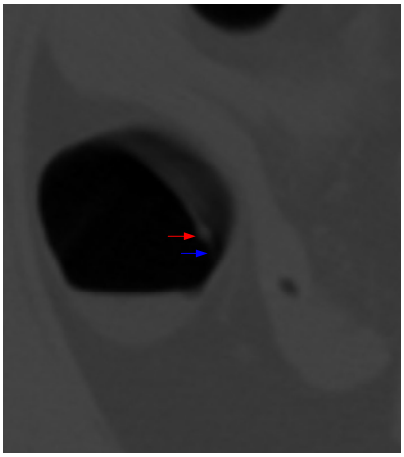

(e)

Figure 2.14 Position in a supine colon corresponding to a suspicious polyp in a prone colon and an estimated polyp position by the proposed method. (a) The two positions viewed inside the colon, (b) The two positions viewed outside the colon (Blue: the estimated position by the proposed method, Red: false positive polyp position), (c) Sagittal scan, (d) Coronal scan and (e) Axial scan.

Estimated location) was 13.77 mm while the averaged DRR (Distance between the radiologist-indicated location and the Rigid transformed location) was 32.02 mm. The precision was also improved by 68.2% (the variance of the DRE was 6.20 mm while the variance of the DRR was 19.51 mm). As discussed in the introduction, a direct comparison for polyp location estimation between our averaged DRE (13.77 mm) and Acar *et al.* [40] and P. Li *et al.* [46] 's error (12.66 mm) is not appropriate. Since P. Li *et al.* did not deal with 3D volume registration, they only registered the colonic central paths, their distance error is calculated on the centerline between the projected polyps on the colonic centerline for both radiologist-indicated polyps and their estimated polyps. Therefore, their errors would likely increase when measured by the DRE criteria. To see the impact of the registration we can construct the following scenario. Suppose that a radiologist locates a polyp in either the supine or the prone data. If the radiologist also finds the polyp at the corresponding area in the other (supine or prone) image, they can improve their confidence that the location is a true positive. By reducing the region of interest to that centered on the corresponding polyp, the proposed registration can increase their confidence in the polyp's classification. For example in Figure 2.14, radiologists found a polyp-like shape at (-87.83, 18.73, -307.53) in a patient's prone colon. The coordinate estimated by our method in the patient's supine colon for that point was (100.94, -16.33, -297.00). The radiologists could search for the polyp-like shape around the estimated point with about 30 mm radius. The real corresponding polyp-like shape was at (88.26, -9.18, -284.00) (Figure 2.14 (a) and (b)) and the difference was 19.51 mm. Figure 2.14 (c), (d) and (e) show the corresponding polyp-like shape found around the estimated point. Using this process, radiologists can increase their confidence about the polyp at that point.

Although we see an increased accuracy of estimating polyp location between scans by 3D non-rigid deformation, the method presented is still not sufficient to directly incorporate image data such as lumen curvature simultaneously into CAPD to detect polyps below the accuracy of the registration.

The registration method presented has an additional limitation in that it can work only when both supine and prone colons are single connected in their shapes, respectively. If one of the supine and prone colons is not single connected, the centerline for that colon volume cannot be adapted to the piecewise centerline matching algorithm. In addition, the extended demons registration method is not reliable when the shapes undergo a topological change.

2.5 Conclusion

We presented a new approach to deformable registration of prone and supine colon volumes. The proposed method consists of two steps. First, we introduce a piecewise centerline matching method, and used a deformation field interpolated and extrapolated from the difference vectors of those piecewise matched regions for the purpose of including the feature information into the registration process. By adding this step to the second extended demons registration method, we could obtain more accurate volume registration results even though one or both of the supine and prone colon volumes have complicated, twisted regions. The second contribution is the extended demons registration method, which uses a level-set representation of the object boundary as inputs to the demons registration algorithm. From this level-set representation, the demons algorithm can register the 3D volumes with high accuracy even though the two objects are separated and minimally overlapping.

We evaluated the proposed method on real patients' supine and prone colon volumes. The registered volumes are well reconstructed and accurate. We also adapted our method to trace the polyp locations in the patients' colons, which were already identified by a radiologist. The supine polyps were estimated from the prone polyps by our proposed method and the estimated polyp locations compared with the radiologist-indicated supine polyp locations.

2.6 Acknowledgment

The authors would like to thank Dr. Pete Santago, Dr. Don Gage, Haiyong Xu and Dr. Yaorong Ge for their valuable suggestions. The authors also gratefully acknowledge the use of patient data from the Wake Forest University School of Medicine and the Virtual Colonoscopy Resource Center. This research was financially supported in part by NIH grant 1R01CA114492-01A2.

CHAPTER 3. REGISTRATION OF PRONE AND SUPINE COLONS IN THE PRESENCE OF TOPOLOGICAL CHANGES

3.1 Abstract

CT colonography is a minimally-invasive screening technique for colorectal polyps in which X-ray CT images of the distended colon are acquired, usually in the prone and supine positions. Registration of segmented colons from both images will be useful for computer-assisted polyp detection. We have previously presented an algorithm [51, 64] for registration of the prone and supine colon when both are well distended and there is a single connected lumen. However due to inadequate bowel preparation or peristalsis there may be collapsed segments in one or both of the colons resulting in a topological change in the images. Such changes make deformable registrations of the colons difficult, and at present there are no registration algorithms which can accommodate them. We present an algorithm which can perform volume registration of prone/supine colon images in the presence of a topological change.

3.2 Introduction

CT colonography (CTC) is a non-invasive technique for detecting colorectal polyps and colon cancer. CTC has several advantages over optical colonoscopy including reduced risk of complications and increased patient compliance within screening recommendations. However, the presence of liquid stool by inadequate bowel preparation makes it difficult to examine the colon lumen for detection of polyps in CTC. The remaining stool may conceal the lower parts of the interior colon when the patients are in the prone or supine positions for CT scanning. Furthermore, the remaining stool may block some parts of the colon lumen, which results in the colon disconnection in the CT image. The colon disconnection by colon collapse in the CT image also occurs by the normal peristalsis of the colon. The registration of prone and supine colons, when one of them has collapsed regions, is both a non-rigid registration problem and a topological problem (because the missing parts of colon in the images cause topological differences). Although the topologically different colon volumes are more frequently observed in the CT colonography than

fully-connected colon volumes, the topological difference problem in CTC has not been studied because it is very hard to deal with the missing information of colonic position and shape.

As a sole previous work to handle topologically different objects in other application, the non-rigid image registration method of Cuzol *et al.* [45] makes use of a scalar vorticity of the motion vector field and divergences for source particles in order to model the non-rigid deformation of lesions in the 2 dimensional brain image. They introduce vorticity for rotating motions in the deformation field, and divergence for the mathematical description of sinks or sources. This divergence term is related to topological change between images. Thus, the deformation field is organized by two sets of vortex and source particles. Although their approach in 2 dimensional brain images is robust enough to deal with topological change of the images, solving the required optimization problem is difficult even in the 2 dimensional case. To extend the method to the 3 dimensional case, it is suggested in their paper [45] that "Because the vorticity is no longer a scalar but a vector, they should consider a line source or a surface source in the 3 dimensional extension instead of a particle source in the 2 dimensional version". The three dimensional extension of this method requires an excessively long execution time based on complex derivation of the mathematical formulations.

In this chapter, we present an algorithm for registration of segmented colons from CT colonography images in the presence of topological shape differences. The algorithm proposed previously ([51, 64]) cannot be applied in cases where there is a topological change in the prone and supine colon shape. The algorithm presented in this chapter has been adapted from applications in neuroimage analysis [65]. For the registration between topologically different objects, the proposed algorithm uses an image evolution of an embedded map representation after rigid transformation of the segmented images.

3.3 Background

For 2 dimensional image registration with topological differences, Wyatt [65] embedded a 2 dimensional image as a manifold in a 3 dimensional space through a mapping $X(x,y):\mathbf{R}^2 \to \mathbf{R}^3$ where,

$$\begin{aligned} X^1(x,y) &= x \\ X^2(x,y) &= y \\ X^3(x,y) &= \sigma I(x,y) \end{aligned} \quad . \qquad (1)$$

The σ value in 2 dimensions means the variation rate of the intensity since the intensity is of a different scale than (x, y) coordinates. The relationship in (1) can be depicted in Figure 3.1. He used the Riemannian metric to measure distance on the surface *X* as below.

$$ds_X^2 = g_{x,x}dxdx + g_{x,y}dxdy + g_{y,x}dydx + g_{y,y}dydy\,, \qquad (2)$$

where the metric tensor is defined by

$$g_{\alpha,\beta} = \sum_{i=1}^{3}\sum_{j=1}^{3} h_{i,j}\frac{\partial X^i}{\partial \alpha}\frac{\partial X^j}{\partial \beta}\,. \qquad (3)$$

and where, $h = \begin{bmatrix} 1 & 0 & 0 \\ 0 & 1 & 0 \\ 0 & 0 & \sigma^2 \end{bmatrix}$.

From (3), $g_{x,x} = 1+\sigma^2 I_x^2$, $g_{x,y} = g_{y,x} = \sigma^2 I_x I_y$, $g_{y,y} = 1+\sigma^2 I_y^2$.

The normal at any point *p* on the surface is given by

$$\mathbf{U}_p = \frac{X_x \times X_y}{\sqrt{g_{x,x}g_{y,y} - g_{x,y}g_{x,y}}} = -\frac{1}{\sqrt{\sigma^2 {I_x}^2 + \sigma^2 {I_y}^2 + 1}}\left[-\sigma I_x, -\sigma I_y, 1\right]^T. \qquad (4)$$

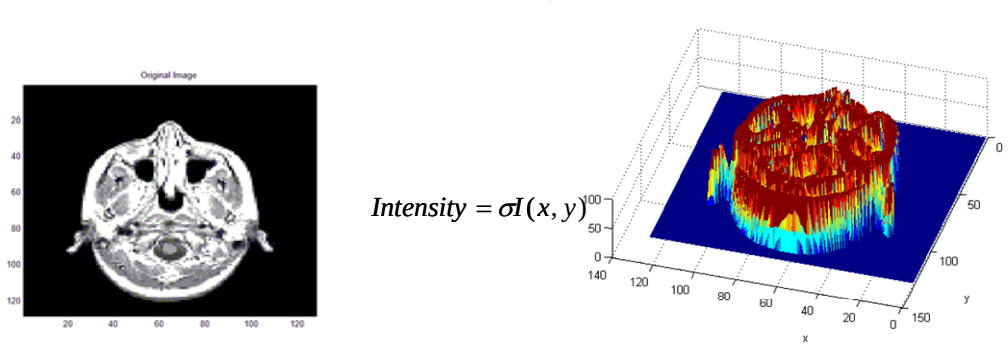

(a) Normal 2D brain image (b) Embedded 2D image as a manifold in 3D space

Figure 3.1. Visualization of the embedded representation of a 2 D image.

U is the normal to the embedded manifold in the Riemannian space. For an image evolution in its normal direction with a given speed ϕ, he set

$$\frac{\partial X}{\partial t} = \phi \mathbf{U} \qquad \text{where} \quad \phi(\vec{x}) = I_T - I(t). \tag{5}$$

After dicretization,

$$\begin{bmatrix} a_{i,j}^{l+1} \\ b_{i,j}^{l+1} \\ c_{i,j}^{l+1} \end{bmatrix} = \begin{bmatrix} a_{i,j}^{l} \\ b_{i,j}^{l} \\ c_{i,j}^{l} \end{bmatrix} + \Delta t \cdot S \begin{bmatrix} -\sigma m(F_x^+, F_x^-) \\ -\sigma m(F_y^+, F_y^-) \\ 1 \end{bmatrix}. \tag{6}$$

Here,

$$F_x^+ = \frac{F_{i+1,j,k} - F_{i,j,k}}{\Delta x}, \quad F_x^- = \frac{F_{i,j,k} - F_{i-1,j,k}}{\Delta x} \quad F_y^+ = \frac{F_{i,j+1,k} - F_{i,j,k}}{\Delta y}, \quad F_y^- = \frac{F_{i,j,k} - F_{i,j-1,k}}{\Delta y}. \tag{7}$$

$$m(\alpha, \beta) = \begin{cases} sign(\alpha)\min(|\alpha|, |\beta|), & if\ \alpha\beta > 0 \\ 0, & if\ \alpha\beta \le 0 \end{cases}. \tag{8}$$

$$S = \frac{-G * (I_T - I_{i,j}^l)}{\left(1 + \sigma^2 m(F_x^+, F_x^-)^2 + \sigma^2 m(F_y^+, F_y^-)^2\right)^{\frac{1}{2}}}. \tag{9}$$

3.4 Methods

Figure 3.2 shows the block diagram for the proposed registration method. In Figure 3.2, the "Feature-based registration by centerline analysis" section is almost the same as in our previous paper [2] except that one of the two colon lumen centerlines is disconnected. As input volumes for the different topology registration, the original single connected colon and an intermediate colon reconstructed by piecewise centerline matched deformation field from original disconnected colon are used. For registration of topologically different images, the algorithm to be presented uses an embedded map representation of the segmented images.

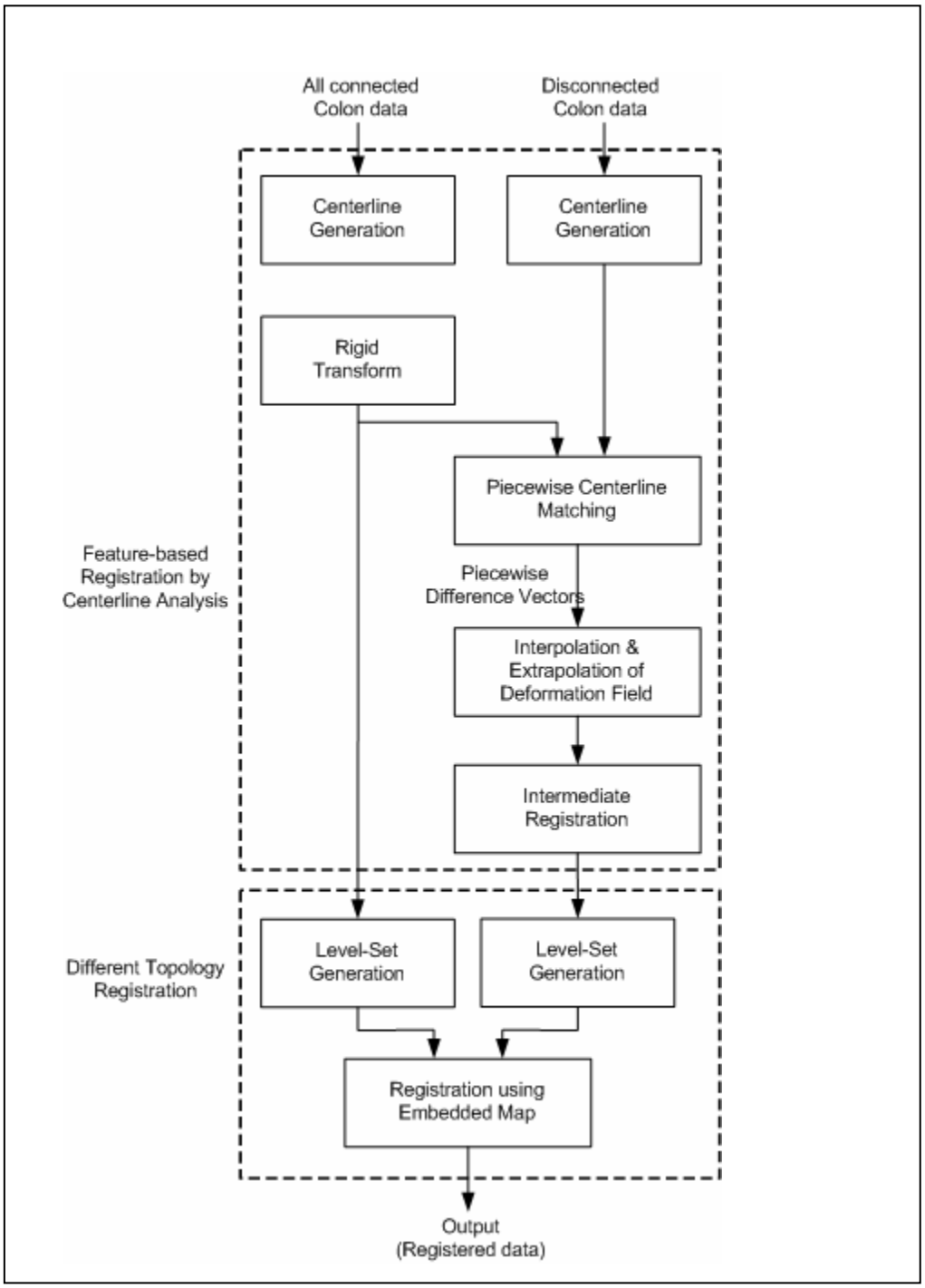

Figure 3.2. Block diagram for proposed registration method

3.4.1 Embedded manifolds for three dimensional space

The images can be embedded as a manifold in a 4D space through a mapping $X(x,y,z):\mathbf{R}^3 \to \mathbf{R}^4$ where

$$\begin{aligned} X^1(x,y,z) &= x \\ X^2(x,y,z) &= y \\ X^3(x,y,z) &= z \\ X^4(x,y,z) &= \sigma I(x,y,z) \end{aligned} \quad . \tag{10}$$

According to Gray [66], the definition for a normal vector, which is perpendicular to several vectors, is as follows. When M is a regular surface in $\mathbf{R}^n$ and $\mathbf{U}_p \in \mathbf{R}^n_{\mathbf{p}}$ with $\mathbf{p} \in M$, $\mathbf{U}_p$ is perpendicular to the regular surface M at p, provided $\mathbf{U}_p \cdot \mathbf{v}_p = 0$ for all tangent vectors $\mathbf{U}_p \in M_p$ [66]. In our application, all tangent vectors are

$$\mathbf{X}_x = \begin{bmatrix} 1 \\ 0 \\ 0 \\ \sigma I_x \end{bmatrix}, \quad \mathbf{X}_y = \begin{bmatrix} 0 \\ 1 \\ 0 \\ \sigma I_y \end{bmatrix}, \quad \mathbf{X}_z = \begin{bmatrix} 0 \\ 0 \\ 1 \\ \sigma I_z \end{bmatrix}. \tag{11}$$

Let's suppose that the normal vector to these tangent vectors is $\mathbf{U}_p = [a,b,c,d]^T$, then

$$\begin{aligned} \mathbf{U}_p \cdot \mathbf{X}_x &= 0 \\ \mathbf{U}_p \cdot \mathbf{X}_y &= 0 \\ \mathbf{U}_p \cdot \mathbf{X}_z &= 0 \end{aligned} \quad . \tag{12}$$

From (12)

$$d\sigma I_x = -a, \qquad d = \frac{-a}{\sigma I_x},$$

$$b = -d\sigma I_y = -\sigma I_y\left(\frac{-a}{\sigma I_x}\right) = \frac{I_y}{I_x}a, \tag{13}$$

$$c = -d\sigma I_z = -\sigma I_z\left(\frac{-a}{\sigma I_x}\right) = \frac{I_z}{I_x}a.$$

$$\therefore \quad \mathbf{U}_p = a\left[1, \frac{I_y}{I_x}, \frac{I_z}{I_x}, \frac{-1}{\sigma I_x}\right]^T = -\frac{a}{\sigma I_x}\left[-\sigma I_x, -\sigma I_{y,} - \sigma I_z, 1\right]^T \quad . \tag{14}$$

After normalization,

$$a = \frac{\sigma I_x}{\sqrt{\sigma^2 {I_x}^2 + \sigma^2 {I_y}^2 + \sigma^2 {I_z}^2 + 1}} \quad , \tag{15}$$

$$\mathbf{U}_p = -\frac{1}{\sqrt{\sigma^2 {I_x}^2 + \sigma^2 {I_y}^2 + \sigma^2 {I_z}^2 + 1}}\left[-\sigma I_x, -\sigma I_{y,} - \sigma I_z, 1\right]^T. \tag{16}$$

Equation (16) is quite similar to that of the normal at any point p on the manifold in 2D [65] except z-element expansion. The time step of the evolution was adapted at each iteration using

$$\Delta t \le \frac{1}{8\max\left(\left|\phi\right| \Big/ \left\|U\right\|\right)} \quad . \tag{17}$$

3.4.2 Image evolution with manifold

For an image evolution in its normal direction with a given speed ϕ, we set

$$\frac{\partial X}{\partial t} = \phi \mathbf{U}, \qquad \text{where} \quad \phi(\vec{x}) = I_T - I(t). \tag{18}$$

From (16),

$$\begin{bmatrix} a(t) \\ b(t) \\ c(t) \\ d(t) \end{bmatrix} = \frac{-\left(I_T - I(t)\right)}{\sqrt{\sigma^2 {I_x}^2 + \sigma^2 {I_y}^2 + \sigma^2 {I_z}^2 + 1}} \begin{bmatrix} -\sigma I_x \\ -\sigma I_{y,} \\ -\sigma I_z \\ 1 \end{bmatrix}. \tag{19}$$

A min/mod finite difference scheme (equation (8)) is used to approximate the derivatives of the current images as in [36]. Gaussian filtering with discrete images $I_{j,k}$, to reduce the sensitivity of the derivatives to noise, and the forward and backward derivative operators of the filtered image $F = G * I$ are used for the discretized equation,

$$\begin{aligned} F_x^+ &= \frac{F_{i+1,j,k} - F_{i,j,k}}{\Delta x}, \quad F_x^- = \frac{F_{i,j,k} - F_{i-1,j,k}}{\Delta x}, \\ F_y^+ &= \frac{F_{i,j+1,k} - F_{i,j,k}}{\Delta y}, \quad F_y^- = \frac{F_{i,j,k} - F_{i,j-1,k}}{\Delta y}, \\ F_z^+ &= \frac{F_{i,j,k+1} - F_{i,j,k}}{\Delta z}, \quad F_z^- = \frac{F_{i,j,k} - F_{i,j,k-1}}{\Delta z}. \end{aligned} \tag{20}$$

The final discretized equation is then

$$\begin{bmatrix} a_{i,j,k}^{l+1} \\ b_{i,j,k}^{l+1} \\ c_{i,j,k}^{l+1} \\ d_{i,j,k}^{l+1} \end{bmatrix} = \begin{bmatrix} a_{i,j,k}^{l} \\ b_{i,j,k}^{l} \\ c_{i,j,k}^{l} \\ d_{i,j,k}^{l} \end{bmatrix} + \Delta t \cdot S \begin{bmatrix} -\sigma m(F_x^+, F_x^-) \\ -\sigma m(F_y^+, F_y^-) \\ -\sigma m(F_z^+, F_z^-) \\ 1 \end{bmatrix} \quad , \qquad (21)$$

where l is the iteration number and,

$$S = \frac{-G*(I_T - I_{i,j,k}^{l})}{\left(1+\sigma^2 m(F_x^+, F_x^-)^2 + \sigma^2 m(F_y^+, F_y^-)^2 + \sigma^2 m(F_z^+, F_z^-)^2\right)^{\frac{1}{2}}} \quad . \qquad (22)$$

3.4.3 Input volume preparation

For an initial 3D experiment, topologically different, synthetic images were used as source and target as shown in Figure 3.3. The source object has an oval shape and the target object has a donut-like shape which is an obviously different topology from that of the source. The dimensions of the source and target object are 50x50x50 pixels. Figure 3.4 shows the resulting object after registration. Although the resulting object is topologically different, it is not a solid object. The resulting object forms a multi-layered object (like an onion) because the input objects undergo a smoothing process by the Gaussian filter G during the registration process. This smoothing process blurs the object boundary. This multi-layered object cannot be used as a result of registration because it is difficult to decide which layer corresponds to original surfaces of the source object and target object. In order to overcome this problem, source and target objects are reconstructed by the level-set representation using a distance map as shown in Figure 3.5. In Figure 3.5, the source object at level=0 shown in Figure 3.5-c and the target object at level=0 shown in Figure 3.5-g represent original surfaces of source object and target object, respectively.

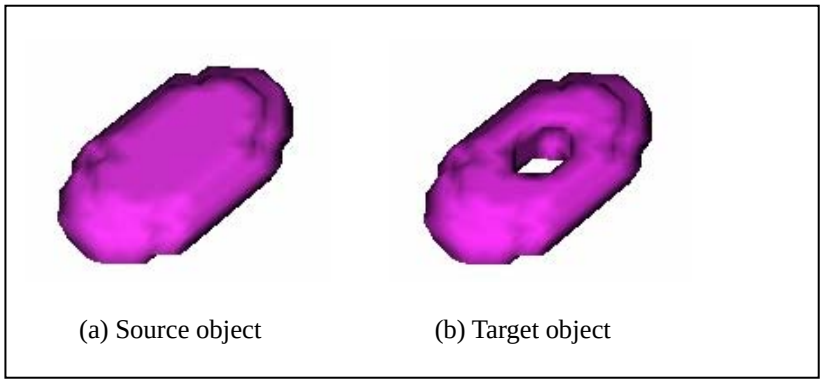

(a) Source object (b) Target object

Figure 3.3 Topologically different source and target object in 3D

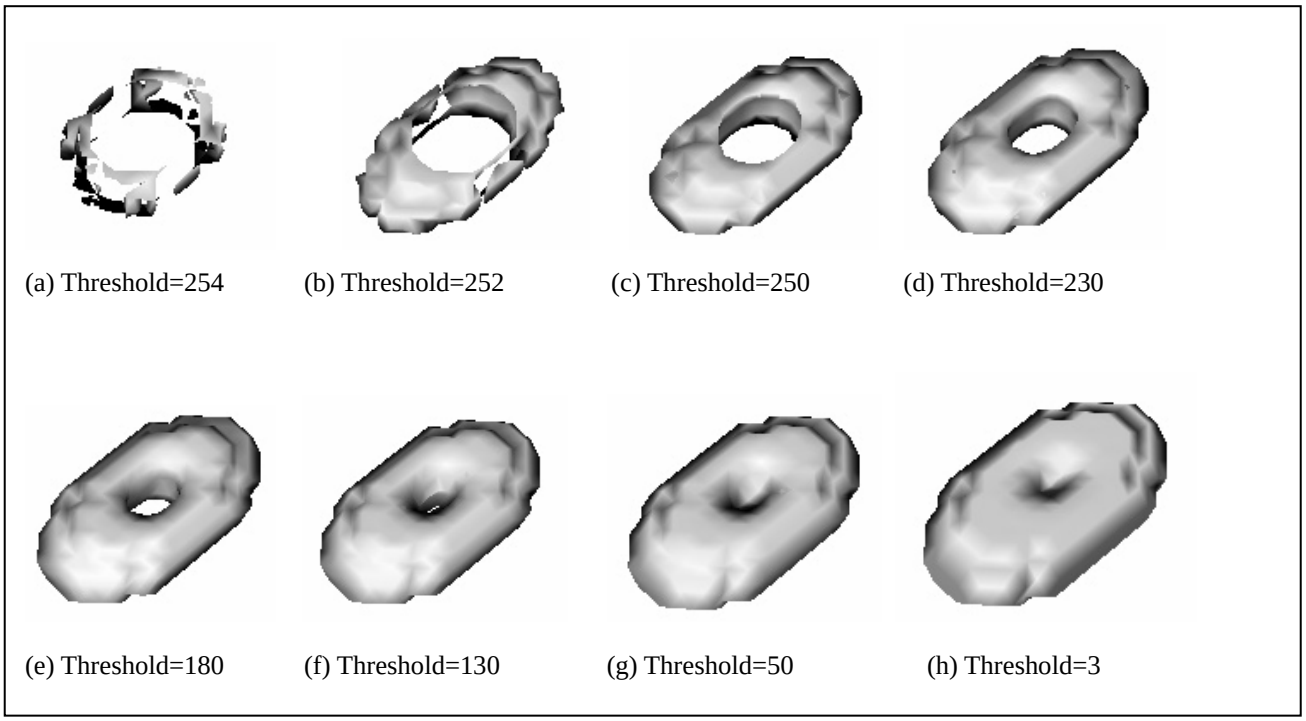

(a) Threshold=254 (b) Threshold=252 (c) Threshold=250 (d) Threshold=230

(e) Threshold=180 (f) Threshold=130 (g) Threshold=50 (h) Threshold=3

Figure 3.4 Registration result: onion-like object which has many layers. ((a)-(h) show the same object with different layer at each threshold value)

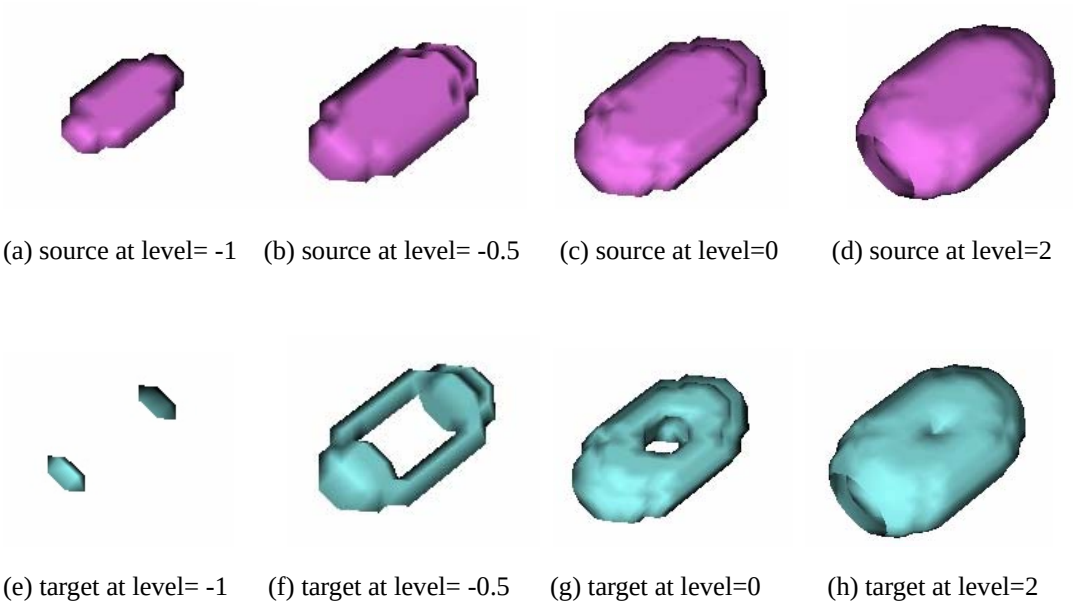

(a) source at level= -1 (b) source at level= -0.5 (c) source at level=0 (d) source at level=2

(e) target at level= -1 (f) target at level= -0.5 (g) target at level=0 (h) target at level=2

Figure 3.5 Level-set representation of source and target objects using distance map

3.5 Results

3.5.1 Results for synthesized volumes

Figure 3.6 shows the registration results using level-set represented inputs. As one can see in Figure 3.6, the oval source object (Figure 3.3-a) is evolved to the donut-like target object (Figure 3.6-c) after 25 iterations at the level=0. In Figure 3.7, another topological difference example is shown. In this example, a big tube-like object is used as a source volume (Figure 3.7-a) and two disjoint tube-like objects are used as a target volume (Figure 3.7-b). Figure 3.8 shows each step of iterations to evolve the source into the target at the level=0.

(a) Registration result at 15 iteration with level=0

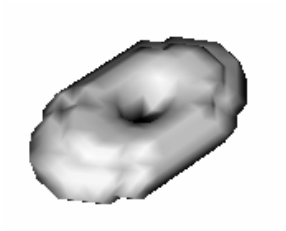

(b) Registration result at 20 iteration with level=0

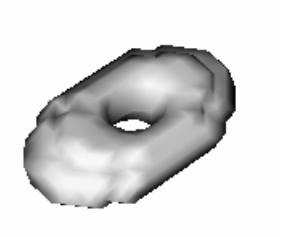

(c) Registration result at 25 iteration with level=0

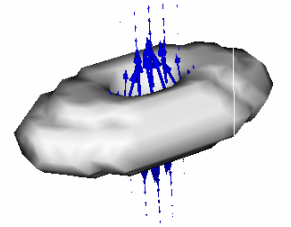

(d) Final registration result after 25 iteration with deformation field

Figure 3.6 The evolution of registration results during iteration ((a)-(c)) and final deformation field (d)

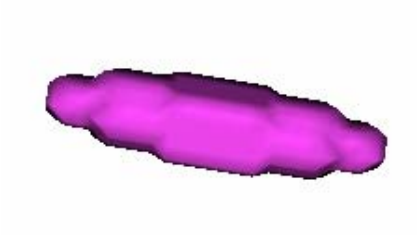

(a) Tube-like object as a source

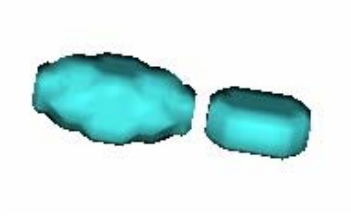

(b) Two tubes as a target

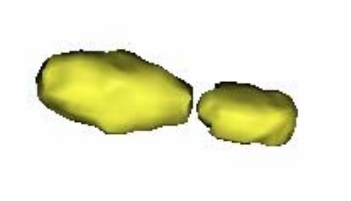

(c) registered results after 28 iterations

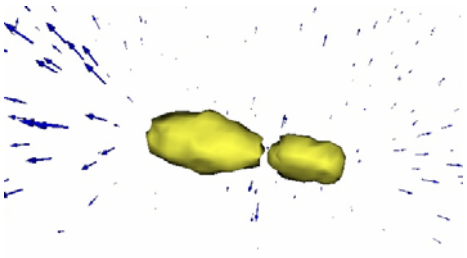

(d) Final registration result after 28 iterations with deformation field

Figure 3.7 Another topologically different source, target object in 3D and their registered result.

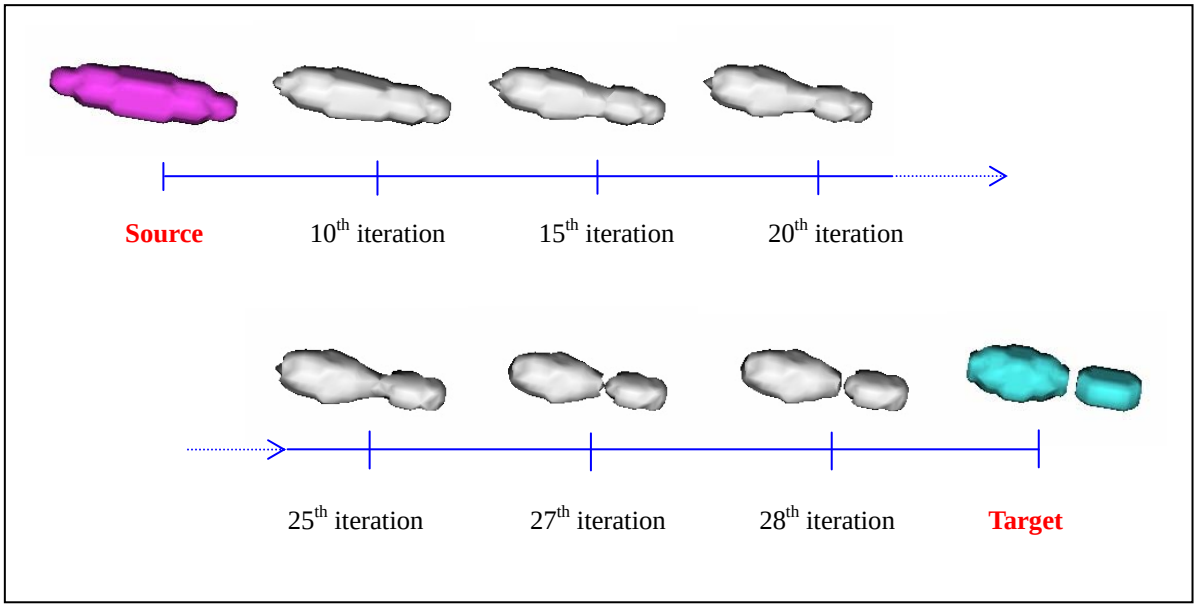

Figure 3.8 The evolution of registration results of Figure 3.7 at various numbers of iterations with level=0

3.5.2 Results for topologically different colons

The figures below show the results applying the proposed method to colon images. Figure 3.9-a is a segmented colon from a patient's prone CT data, which is well distended and all connected. Figure 3.9-b is a segmented supine colon data of the same patient but disconnected due to the insufficient distention. Figure 3.9-c is an intermediate colon registered from Figure 3.9-b using the piecewise centerline matched deformation field. Figure 3.9-d is the final registered colon from the intermediate colon (Figure 3.9-c) after the application of the 4D deformation field. The final registered volume of Figure 3.9-d is quite similar to the target volume of Figure 3.9-a even though the source (Figure 3.9-b) is topologically different. Figure 3.9-e and 3.9-f display the final registered colon from the intermediate colon (Figure 3.9-c) by three dimensional deformation field except 4^{th} embedded map representation and its three dimensional deformation field. Without the 4^{th} embedded map representation, the final reconstructed volume of the three dimensional result shows that it still has a disconnected region. Estimating polyp location between supine and prone colons would be calculated by only the three dimensional deformation field (Figure 3.9-f) without 4^{th} component of embedded map representation while the registered colon volume is reconstructed by whole embedded representation. Figure 3.10 shows the polyp estimation result using only the three

dimensional deformation field. The blue point in the Figure 3.10-a indicates an original polyp location in the single connected colon.

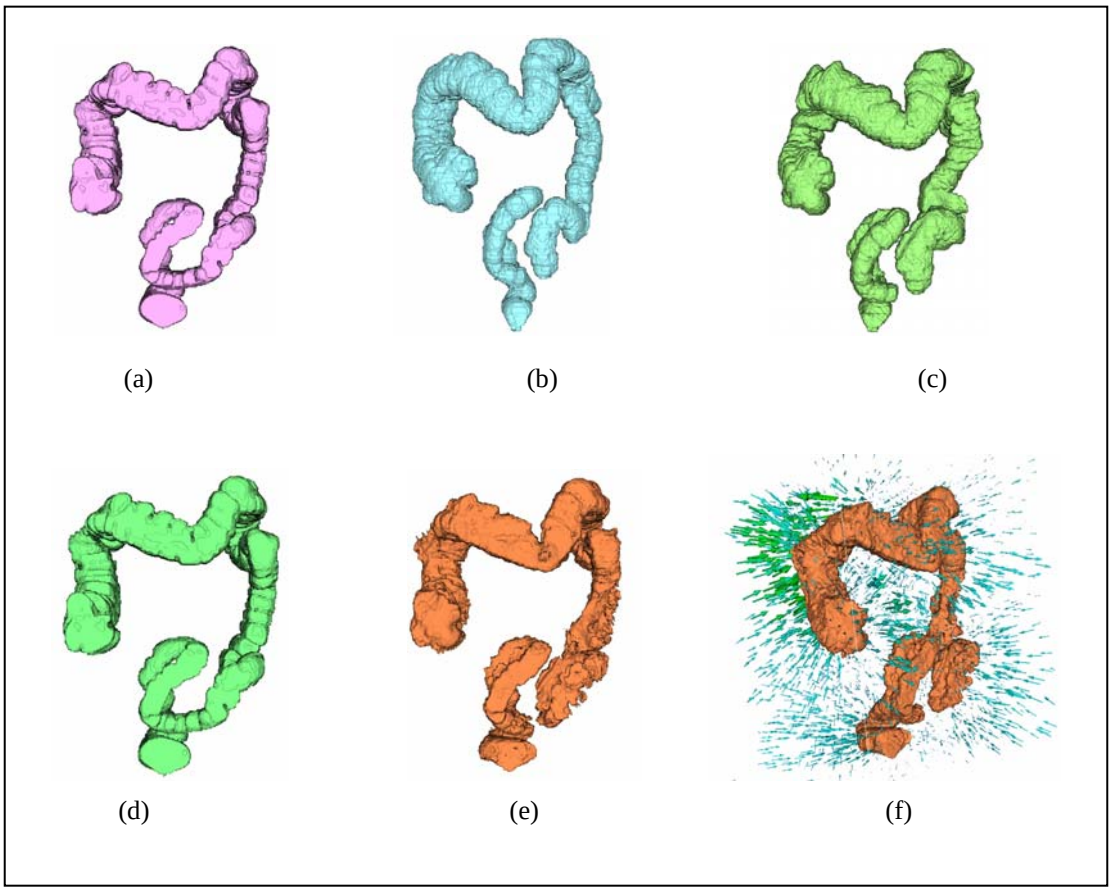

Figure 3.9 Registration of topologically different colon images: (a) all connected target colon, (b) topologically different source colon, (c) intermediate colon reconstructed by piecewise centerline matched deformation field from (b), (d) final registered colon by 4 dimensional deformation field based on embedded map, (e) final registered colon by three dimensional deformation field except 4^{th} embedded map and (f) three dimensional deformation field for (e).

Another blue point in Figure 3.10-b is the registered polyp location from the polyp location (blue point in Figure 3.10-a) in the single connected colon by the deformation field of proposed method, and red point in the Figure 3.10-b is its corresponding original polyp location in the disconnected colon. The distance error between the original polyp location (red point in Figure 3.10-b) and its

registered polyp location (blue point in Figure 3.10-b) is 34.69 mm while the distance error between the original polyp location and simple rigid-transformed polyp from the single connected colon is 52.65 mm.

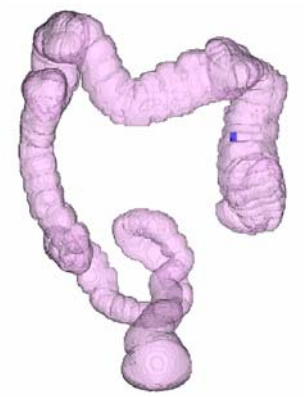

(a) Original polyp location (blue point) in the single connected colon

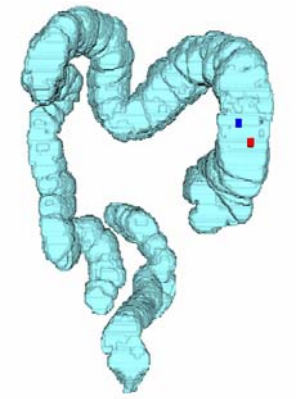

(b) Registered polyp location (blue point) from the polyp location in (a) and its corresponding polyp location (red point) in a disconnected colon.

Figure 3.10 Polyp estimation using three dimensional deformation field

3.6 Discussion

The physical significance of the 4th component in embedded map representation is adding or peeling out the real surface of the object volume. It is a kind of working with clay or play-doh™ like Figure 3.11 while the first three components of the embedded map representation are the normal three dimensional deformation field.

(a) play-doh™

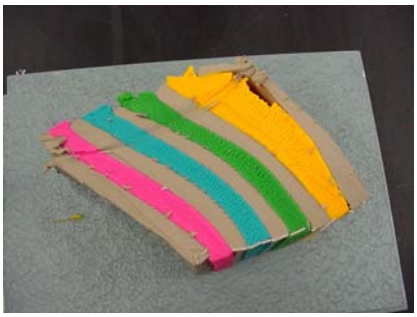

(b) Several layers representing the added surface for the 4th component of embedded map in 3D

Figure 3.11 Multi-layers with play-doh™ for representing the 4th component of the embedded map in 3D

Thus, theoretically the source volume can evolve into the target volume with almost zero values of the first three components and the dominant 4th component depending on the σ value in Equation (8) and (19). This means that the source object can evolve into the target by only carving and adding the source surface without moving the source object voxels. This is not a desirable situation from the registration point of view because the registration process is required to know the spatial transformation which is directly related to the first three components.

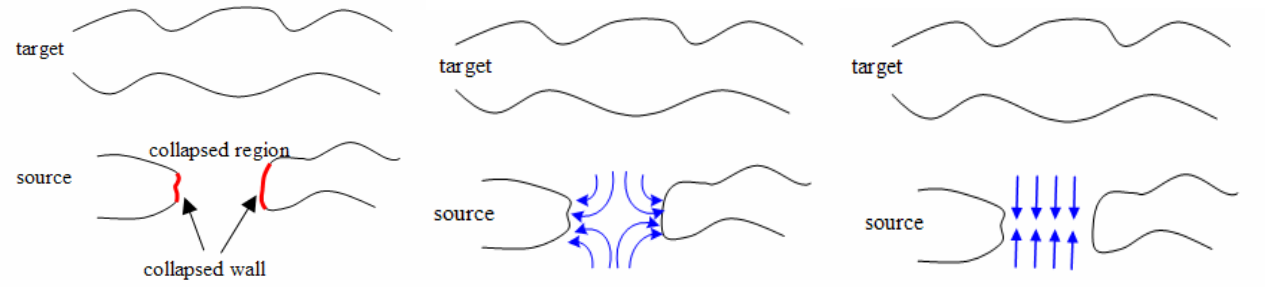

(a) (b) (c)

Figure 3.12 Relation between a collapsed colon region and its corresponding region. (a) collapse region in source colon, (b) source collapsed wall matched with target colon lumen and (c) collapsed region filled with layers of different dimension.

The value $\sigma = 2$ value was found experimentally to obtain reasonable results for the first three components. In case of a collapsed region in the disconnected colon and the corresponding region in the single connected colon, there might be two different deformable matching methods. The first is that the vertical walls in the collapsed region are matched to some points of the colon lumen of the single connected colon as shown in Figure 3.12-b. Note that, this matching result is purely mathematical and is far from reality because the collapsed region is actually missing information due to inadequate distention of colon or remaining stool within colon. Hence, there is no part in the single connected colon that corresponds to the collapsed region, and reconstructed colon lumens suffer from the same inaccuracy. But, the second proposed embedded map representation fills the collapsed region in the colon with a totally new layer from another dimension (Figure 3.12-c). Thus, the proposed attempt using the embedded map representation reflects the physical situation more realistically.

In the polyp estimation result, the distance error (34.69 mm) between the original polyp location (red point in Figure 3.10-b) and its registered polyp location (blue point in Figure 3.10-b) tends to be larger than the average distance error (13.77 ± 6.20 mm) of the centerline analysis with the extended demons algorithm in Chapter 2.

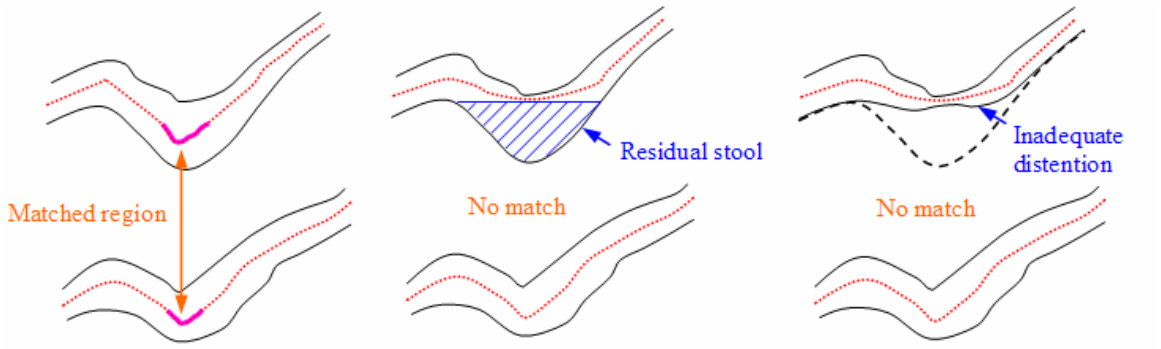

Figure 3.13 Feature matching errors by centerline distortion (a) correctly matched region by extrema of centerline, (b) no match by centerline analysis due to the residual stool, (c) no match by centerline analysis due to inadequate distention.

One of the reasons for the larger distance error of polyp estimation is that the volume change by 4^{th} element of embedded map representation is not taken into consideration on estimating polyp location. Polyp estimation was performed only by the three dimensional deformation field. Another reason is that the disconnected colon volumes tend to have more severely deformed regions caused by inadequate distention and residual stool, which affect the piecewise centerline matching results as shown in Figure 3.13. As described in Chapter 2, anatomically similar regions in the shape of the colon can be more clearly exposed by the colon centerline. Thus, the piecewise centerline matched regions between supine and prone colons play an important role in increasing the accuracy of registration by propagating the difference vectors on the matched centerline pieces. As one can see in Figure 3.13, the correctly matched region (Figure 3.13-a) found by extrema of the centerline may not be correctly detected when there are severe distortions of the colon lumen by residual stool (Figure 3.13-b) or inadequate distention (Figure 3.13-c) or both.

3.7 Conclusion

This paper presents an algorithm for registration of segmented colons from CT colonography images when there is a topological difference between the shapes. This occurs when there is a collapsed segment during shifting of the patient between acquisitions. Deformable registration of images undergoing topological change is a relatively unexplored aspect of registration, but one that is important in real world imaging situations, as the application to CT colonography shows.

This topological difference of reconstructed colon volume makes it very difficult to detect the polyp from the fully automated analysis of the colon. Therefore, the proposed colon registration method which can deal with topological problems of the colon images will contribute to practical use of CT colonoscopy in clinical situations.

CHAPTER 4. CONCLUSION

CT colonography has many advantages that make it an attractive diagnostic tool for detecting colorectal polyps. The previous chapters have shown some clinical limitations of CT colonography (CTC) and how CTC can be improved by 3D volume registration.

In Chapter 2, the registration method for topologically consistent images combined a feature-based centerline matching method with an extended demons algorithm that uses a level-set representation. After rigid transformation based on the patient's anus point, a feature-based registration is used to align the lumens approximately about their centerlines, defining an initial non-linear deformation field. Features, anatomically similar regions in the shapes of the two colons, are calculated by piece-wise centerline analysis. The initial estimation of the deformation field is refined using the extended demons algorithm. As a volume-based deformation registration, the extended demons algorithm is more efficient for both binary objects and little-overlapping objects than the original demons algorithm. As shown by the validation study, the combined method can register topologically consistent lumens with Jaccard similarity coefficients of 0.915 ± 0.07 over 21 datasets. When compared with results by rigid transform alone, this method demonstrates increased polyp corroboration accuracy.

In Chapter 3, the registration algorithm designed for topologically different images combined the centerline method discussed previously with an embedded map representation of the segmented colons. This method is also effective when used with images that exhibit non-tubular (e.g., Donut shaped) topological changes. As pointed out in the introduction, image registration in cases where there is a topological change in the images is difficult, since the images cannot be aligned with just a purely geometric transformation. In CTC, this situation occurs when peristalsis, insufficient distention, or inadequate bowel preparation cause the lumen to be split into multiple air-filled regions. There have been relatively few attempts to handle registration under topological change in any application and none in CTC. Those that have been proposed in neuroimaging have severe computational demands when applied in 3D. Thus the embedded map registration algorithm presented in Chapter 3 for registering lumens' with topological differences represents a new branch of registration methods. However, this method has its limitations such as the difficulty in matching centerlines in the case of a topological change, a prerequisite to applying the embedded map registration method. Future work on the CTC registration problem should focus on this step of approximate matching of centerlines for the embedded map registration method to have higher

accuracy in practical application.

In conclusion, this dissertation has introduced methods for registration of topologically consistent and inconsistent CT colonography images. Through this study, deformable registration for 3D colon volumes was implemented. This enabled the estimation of 3D polyp location between the source (prone) and target (supine) colons within errors of 34.69 mm. Registration of topologically different objects is a common problem in many imaging applications including CTC and this dissertation is one of the earliest to propose an algorithm for this problem. The algorithms introduced in this dissertation can be extended for use in other computer-aided diagnosis (CAD) applications that deal with long tubular regions (eg. virtual bronchoscopy and virtual angioscopy).

This paragraph discusses some suggestions for future direction of this thesis. First is reduction of computation time for the entire registration process by optimization. As mentioned in Chapter 2, almost three hours were needed for the registration of the subsampled (256×256×170) colon data. Thus software structure changes for adapting parallel processing in multi-processor computer can be considered for reducing the computational time. Second is automation of the entire registration process. Currently, there are some parts that require manual setting in both topologically consistent registration and topologically different registration, eg. setting a starting point of centerline and finding patient's anus point for initial rigid transform. These instances of user-intervention in the software could be replaced with a fully automatic registration process. Third is devising other methods which increase the accuracy of estimating polyp location in the topologically different case. As mentioned in Chapter 3, polyp estimation was performed only by the three dimensional deformation field, which is one of the reasons for the larger distance error of polyp estimation. One possible approach to improve this error is adding an approximation of 4^{th} element of embedded map representation into the three dimensional deformation field. The source and target objects are represented as level-sets, and the variation in the 4^{th} component of the embedded map represents adding or peeling out the real surface of the object. Therefore, the perturbation to the surface-normal direction on the real surface (which is reconstructed from only the three dimensional deformation field) may reduce the error. Fourth future direction is the extension of the proposed method to the more complicated colon pairs such as both prone and supine colons have collapsed regions or multiple collapsed regions (Figure 4.1).

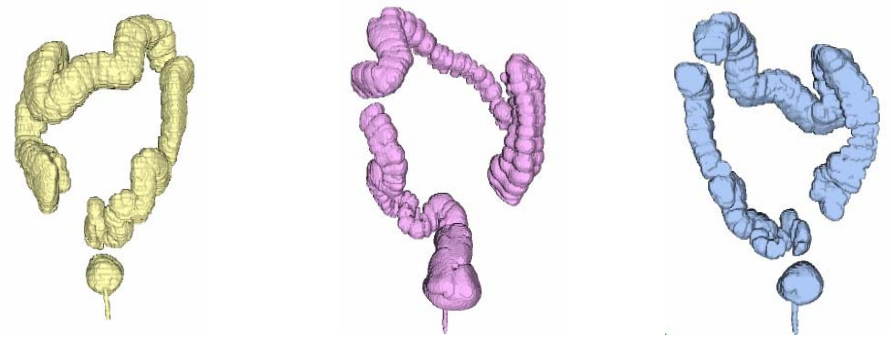

(a) Disconnected supine colon (b) Disconnected prone colon (c) Multiple collapsed colon

Figure 4.1 Examples for more complicated colons

BIBLIOGRAPHY

[1] Parker S, Tong T, Bolden S, Wingo P.,"Cancer statistics 1997", *Cancer Journal for Clinicians*, vol. 47, pp.5-27, 1997.

[2] "ACS Cancer Facts and Figures", *American Cancer Society*, Atlanta. GA. 2002.

[3] D. Ransohoff and C. Lang, "Screening for colorectal cancer", *New England Journal of Medicine*, vol. 325, pp.37-41, 1991.

[4] American College of Radiology Imaging Network (ACRIN) Protocol 6664, July 7, 2006.

[5] Joseph V. Hajnal, Derek L.G. Hill, David J. Hawkes, "Medical Image Registration", *CRC press*, pp.12

[6] http://www.cdc.gov/cancer/screenforlife/terms.htm

[7] http://digestive.niddk.nih.gov/ddiseases/pubs/colonpolyps_ez/

[8] Muhammad A. Butt and Petros Maragos, "Optimum Design of Chamfer Distance Transform", *IEEE Transactions on Image Processing*, vol. 7, No. 10, Oct. 1998.

[9] A. A. Dezin, "Multidimensional Analysis and Discrete Models", pp. 24, CRC Press, 1995

[10] Rosenfeld, A., Pfaltz, J.L., "Sequential Operations In Digital Picture Processing", *Journal ACM* 12 (4), pp.471-494, 1966.

[11] P. A. Lefere, S. S, Gryspeerdt, J. Dewyspelaere, M. Baekelandt and B. G. Van Holbeeck, "Dietary Fecal Tagging as a Cleansing Method before CT Colonography: Initial Results – Polyp Detection and Patient Acceptance", *Radiology*, vol. 224, pp. 393-403, 2002.

[12] Borgefors, G., "Distance Transform in Arbitrary Dimensions", *Computer vision, graphics and image processing*, vol. 27, pp.321-345, 1984.

[13] Y. Zhou and A. Toga, "Efficient Skeletonization of Volumetric Objects", *IEEE Transactions on Visualization and Computer Graphics*, vol. 5, pp. 196-209, July/Sept. 1999.

[14] D. Chen, B. Li, Z. Liang, M. Wan, A. Kaufman and M. Wax, "A Tree-branch Searching Multiresolution Approach to Skeletonization for Virtual Endoscopy", *Proceedings of SPIE Medical Imaging*, vol. 3979, pp. 726-734, 2000.

[15] A. E. Kaufman, S. Lakare, K. Kreeger and I. Bitter, "Virtual Colonoscopy", *Communications of the ACM*, vol. 48, no. 2, pp.38-41, February, 2005.

[16] P. J. Pickhardt, "CT colonography (virtual colonoscopy) for primary colorectal screening: challenges facing clinical implementation", *Abdominal Imaging*, vol. 30, pp.1-4, 2005.

[17] M. Wan, Z. Liang, Q. Ke, L. Hong, I. Bitter and A. Kaufman, "Automatic Centerline

Extraction for Virtual Colonoscopy", *IEEE Transactions on Medical Imaging*, vol. 21, no. 12, December, 2002.

[18] C. L. Wyatt, Y. Ge and D. J. Vining, "Automatic segmentation of the colon for virtual colonoscopy", *Computerized Medical Imaging and Graphics*, vol 24, pp.1-9, 2000.

[19] L. Hong, S. Muraki, A. Kaufman, D. Bartz and T. He, "Virtual Voyage: Interactive Navigation in the Human Colon", *Computer Graphics Proceedings*, SIGGRAPH 97. ACM. pp.27-34, 1997.

[20] E. G. McFarland, "Reader strategies for CT colonography", *Abdominal Imaging*, vol. 27, pp.275-283, 2002.

[21] H. Frimmel, J. Nappi and H. Yoshida, "Fast and robust computation of colon centerline in CT colonography", *Medical Physics*, vol. 31, pp.3046-3056, November 2004.

[22] R. M. Summers, "Challenges for computer-aided diagnosis for CT colonography", *Abdominal Imaging*, vol. 27, pp.268-274, 2002.

[23] Fletcher JG, Johnson CD, Welch TJ, *et al.*, "Optimization of CT colonography technique: prospective trial in 180 patients", *Radiology*, vol. 216, pp.704-711, 2000.

[24] H. Blum, "A transformation for extracting new parameter of shape", in Models for the perception of Speech and Visual Form. Cambridge, MS: MIT Press, 1967.

[25] M.S. Hassouna and A.A. Farag, "Robust Centerline Extraction Framework Using Level Sets" *Computer Vision and Pattern Recognition 2005*, IEEE Computer Society Conference on vol. 1, pp.458 – 465, June 2005

[26] Robert J.T. Sadleir and P.F. Whelan "Colon centreline calculation for CT colonography using optimised 3D topological thinning" *3DPVT 2002* -The first international symposium on 3D data processing visualisation and transmission, Padova, Italy, June 2002.

[27] L. Hong, A. Kaufman, Y. Wei, A. Viswambharn, M. Wax and Z, Liang, "3-D virtual colonoscopy", *Proceedings of Symposium on Biomedical Visualization*, pp. 26-32, 1995.

[28] S. Bouix, K. Siddiqi and A. Tannenbaum, "Flux driven fly throughs", *Computer Vision and Pattern Recognition*, pp.449-454, June 2003.

[29] Y. Ge, D. Stelts, J. Wang and D. Vining, "Computing the centerline of a colon: A robust and efficient method based on 3-D skeleton", *Journal of Computer Assisted Tomography*, vol. 23, no. 5, pp. 786-794, 1999.

[30] M.S. Hassouna and A.A. Farag, "PDE-based Three Dimensional Path Planning for Virtual Endoscopy", *Information Processing in Medical Imaging 2005* LNCS 3565 : pp.176-183, 2005

[31] T. Deschamps and L. Cohen, "Fast extraction of minimal paths in 3D images and applications to virtual endoscopy", *Medical Image Analysis*, vol. 5, pp.281-299, 2001.

[32] I. Bitter, M. Sato, M. Bender, K. McDonnel, A. Kaufman and M. Wan, “CEASAR: A smooth, accurate and robust centerline-extraction algorithm”, *Proceedings of Visualization 2000*, pp.45-52

[33] I. Bitter, A. Kaufman and M. Sato, “Penalized-distance volumetric skeleton algorithm”, *IEEE Transactions on Visualization and Computer Graphics*, vol. 3, pp. 195-206, July/Sept. 2001.

[34] Y. Ge, D. Stelts and D. Vining, “3-D skeleton for virtual colonoscopy”, *Proceedings of 4th International Conference of Visualization in Biomedical Computing*, pp. 449-454, 1996

[35] D. Paik, C. Beaulieu, R. Jeffery, G. Rubin and S. Napel, “Automatic flight path planning for virtual endoscopy”, *Medical Physics*, vol. 25, no. 5, pp. 629-637, 1998.

[36] Vemuri, B. C., Ye, J., Chen, Y., and Leonard, C. M. “Image registration via level-set motion: Applications to atlas-based segmentation”, *Medical Image Analysis*, vol. 7, no. 1, pp. 1-20, 2003.

[37] Vemuri, B. C., Shuangying, H., Sahni, S., Leonard, C. M., Mohr, C., Gilmore, R., and Fitzsimmons, J. “An effcient motion estimator with applications to medical image registration”, *Medical Image Analysis*, vol. 2, no. 1, pp.79-98, 1998.

[38] B.M. Dawant, “Non-rigid registration of medical images: Purpose and methods, a short survey”, *2002 IEEE International Symposium On Biomedical Imaging, Proceedings*, pp.465-468, 2002.

[39] S.Y. Tang, J.Z. Wang and T.Z. Jiang, “Non-rigid registration of medical image using alpha B-spline transformation”, Medical Imaging 2003: Image Processing, *Proceedings ff The Society Of Photo-Optical Instrumentation Engineers* (SPIE) pp.1064-1071, Part 1-3, 2003.

[40] B. Acar, S. Napel, D.S. Paik, P. Li, J.Yee, R.B. Jeffrey and C.F. Beaulieu, “Medial Axis Registration of Supine and Prone CT Colonography Data”, *2001 Proceedings of the 23rd Annual EMBS international Conference*, pp.2433-2436, 2001.

[41] F. B. Nicholson, S. Taylor, S. Halligan and M.A. Kamm, “Recent developments in CT colonography”, *Clinical Radiology*, vol. 60, pp. 1-7, 2005.

[42] G. Iordanescu and R. M. Summers, “Automated Centerline for Computed Tomography Colonography”, *Academic Radiology*, vol.10, no. 11, pp. 1291-1301, Nov, 2003.

[43] Mani A., Napel S., Paik D.S., Jeffrey R.B., Yee J., Olcott E.W., Prokesch R., Davila M., Schraedley-Desmond P. and Beaulieu C.F. “Computed tomography colonography - Feasibility of computer-aided polyp detection in a "First reader" paradigm”, *Journal of Computer Assisted Tomography*, vol. 28, no. 3, pp. 318-326, MAY-JUN, 2004.

[44] J.Z. Liang, W.E. Higgins, R.M. Summers and H. Yoshida, “Introduction to the Special Section on Virtual Endoscopy”, *IEEE Transactions on Medical Imaging*, vol. 23, no. 11, November 2004.

[45] A. Cuzol, P. Hellier and E. Memin, “A Novel Parametric Method for Non-rigid Image

Registration”, *Information Processing in Medical Imaging 2005* LNCS 3565 : pp.456-467, 2005.

[46] P. Li, S. Napel, B. Acar, D.S. Paik, R.B. Jeffrey Jr.and C.F. Beaulieu, “'Registration of central paths and colonic polyps between supine and prone scans in computed tomography colonography: Pilot study”, Medical Physics, Vol. 31 no.10, pp. 2912-2923, OCT. 2004.

[47] J. P. Thirion, “Image matching as a diffusion process: an analogy with Maxwell's demons”, *Medical Image Analysis*, vol. 2, no. 3, pp. 243-260, 1998.

[48] Luis Ibanez, William Schroeder, Lydia Ng and Josh Cates, “ITK Software Guide” , *National Library of Medicine Insight Segmentation and Registration Toolkit* (ITK), Kitware, 2005.

[49] Kitware Inc., “VTK User's Guide”, *Visualization Toolkit* (VTK), Kitware, 2006.

[50] Amy Henderson Squillacote, “Paraview Guide”, ParaView: Parallel Visualization Application, Kitware, 2006.

[51] J. W. Suh and C. L. Wyatt, “Deformable Registration of Prone and Supine Colons for CT Colonography”, *2006 Proceedings of the 28th Annual EMBS International Conference*, pp. 1997-2000, 2006.

[52] D. Shen and C. Davatzikos, "HAMMER: Hierarchical Attribute Matching Mechanism for Eleastic Registration", *IEEE Transactions on Medical Imaging*, vol. 21, no. 11, Nov., 2002.

[53] D. J. Vining, "Virtual endoscopy: is it reality?”, *Radiology*, Vol. 200, pp. 30-31, 1996.

[54] T. Parkins, "Computer lets doctor fly through the virtual colon", *Journal of the National Cancer Institute*, Vol. 86, pp. 1046-1047, 1994.

[55] A.K. Hara, C.D. Johnson, J.E. Reed, R.L. Ehman and D.M. Ilstrup, "Colorectal polyp detection with CT colonography: 2D versus 3D techniques-work in progress", *Radiology*, Vol. 200, pp. 49-54, 1996.

[56] *American College of Radiology Imaging Network* (ACRIN) http://www.acrin.org/6664_ protocol.html

[57] H. Yoshida, F. Nappi, P. MacEneaney, D.T. Rubin and A.H. Dachman, "Computer-Aided Diagnosis Scheme For Detection Of Polyps At CT Colonography", *Radio Graphics*, Vol. 22, No. 4, pp. 963-979, 2002.

[58] J. Yee, N. N. Kumar, R. K. Hung, G.A. Akerkar, P.R.G. Kumar and S.D. Wall, "Comparison of Supine and Prone Scanning Separately and in Combination at CT Colonography", *Radiology*, Vol. 226, no.3, pp.653-661, 2003.

[59] A.H. Dachman, J.K. Kuniyoshi, C.M. Boyle, Y. Samara, K.R. Hoffmann, D.T. Rubin and I. Hanan, "CT colonography with three-dimensional problem solving for detection of colonic polyps", *American Journal of Roentgenology*, Vol. 171, pp.989-995, 1998.

[60] H. Yoshida and A.H. Dachman, "Computer-Aided Diagnosis For CT Colonography", *Semin Ultrasound CT*, 25 (5): pp.419-431 Oct. 2004.

[61] R.E. van Gelder, J. Florie and J. Stoker, "CT Colonography: Practical Aspects and Present Status", *Imaging Decisions MRI*, Vol. 7, pp. 4-9, Oct. 2003.

[62] H. Frimmel, J. Nappi and H. Yoshida, "Centerline-based colon segmentation for CT colonography", *Medical Physicis*, Vol. 32, no. 8, pp. 2665-2672, Aug. 2005.

[63] A.H. de Vries, R. Truyen, J. van der Peijl, J. Florie, R.E. van Gelder, F. Gerritsen, and J. Stoker, "Feasibility of automated matching of supine and prone CT-colonography examinations", *British Journal of Radiology*, Vol. 79, pp.740-744, 2006.

[64] J. W. Suh and C. L. Wyatt, Deformable Registration of Supine and Prone Colons Using Centerline Analysis, *Proceedings of IEEE International Symposium on Biomedical Imaging*, pp. 708-711, April 2007.

[65] C. L. Wyatt and P. J. Laurienti, Nonrigid Registration of Images with Different Topologies using Embedded Maps, *Proceedings of IEEE Engineering in Medicine and Biology Conference*, August 2006.

[66] A. Gray, “Modern Differential Geometry of Curves and Surfaces with MATHEMATICA”, p.288, 2nd edition, 1998, CRC Press.

[67] S.C. Chen, D.S. Lu, J.R. Hecht and B.M. Kadell,"CT colonography: value of scanning in both the supine and prone positions", *American Journal of Roentgenology*, Vol. 172, pp.595-599, 1999.

[68] N. Paragios, M. Rousson and V. Ramesh, "Non-rigid registration using distance functions", *Computer Vision and Image Understanding*, Vol. 89, pp.142-165, 2003

[69] S. Lavallee and R. Szeliski, "Recovering the Position and Orientation of Free-Form Objects from Image Contours Using 3D Distance Maps", *IEEE Transactions on Pattern Analysis and Machine Intelligence*, Vol. 17, no. 4. pp.378-390. 1995

[70] D. Kozinska, O. Tretial, J. Nissanov and C. Ozturk, "Multidimensioanl alignment using the Euclidean distance transform", *Graphical Models Image Process*, Vol. 59, no. 6, pp. 373-385, Nov. 1997.

[71] Virtual Colonoscopy Resource Center. http://www.vcscreen.com/

[72] P.J. Pickhardt, J.R. Choi, I. Hwang, J.A. Butler, M.L. Puckett, H.A. Hildebrandt, R.K. Wong, P.A. Nugent, P.A. Mysliwiec and W.R. Schindler, "Computed Tomographic Virtual Colnoscopy to Screen for Colorectal Neoplasia in Asymptomatic Adults", *New England Journal of Medicine*, Vol.349, No. 23, Dec. 4, 2003.

[73] R. L. Sharma, “Network Topology Opimization”, pp.8, Van Nostrand Reinhold, 1990.

[74] P. A. Burrough, “Principles of Geographic Information Systems for Land Resource Assessment. Monographs on Soil and Resources Survey”, no.12, *Oxford Science Publications*, New York.,1986.

[75] F. L. Bookstein, “Thin-plate splines and the atlas problem for biomedical images”, *Information Processing in Medical Imaging: Proceeding 12th International Conference (IPMI 91)*, pp. 326-342, 1991.

[76] A. Goshtasby, “Registration of images with geometric distortions”, *IEEE Transactions on Geoscience and Remote Sensing*, vol. 26, pp.60-64, 1988.

[77] C. A. Davatzikos, J. L. Prince and R. N. Bryan, “Image registration based on boundary mapping”, *IEEE Transactions on Medical Imaging*, vol. 15, no. 1, pp. 112-115, 1995.

[78] P. Thompson and A. W. Toga, “A surface-based technique for warping three dimensional images of the brain”, *IEEE Transactions on Medical Imaging*, vol. 15, no. 4, pp. 402-417, 1996.

Scholastic Vita

Jung Wook Suh

EDUCATION

Ph.D. in Electrical and Computer Engineering with a Biomedical Option, 2007
Virginia Polytechnic Institute and State University,
Blacksburg, Virginia, U.S.A

M.S. in Electronic Communication Engineering, 1998
Hanyang University,
Seoul, Korea

B.S. in Electronic Communication Engineering, 1996
Hanyang University,
Seoul, Korea

PUBLICATIONS

Journals

- J.W. Suh and J. Jeong, “Fast Sub-pixel Motion Estimation Techniques Having Lower Computational Complexity,” *IEEE Transactions on Consumer Electronics*, Vol. 50, Issue: 3, pp. 968-973, Aug. 2004

- J.W. Suh and J. Jeong, “Model-Based Subpixel Motion Estimation for Image Sequence Compression”, *IEEK (The Institute of Electronics Engineers of Korea*, pp. 130-139, Jan. 1998.

Conference Proceedings

- J.W. Suh and C.L.Wyatt, “Deformable Registration of Supine and Prone Colons using Centerline Analysis”, *2007 International Symposium on Biomedical Imaging*, pp. 708-711, April, 2007

- J.W. Suh and C.L.Wyatt, “Deformable Registration of Prone and Supine Colons for CT

Colonography", *2006 Proceedings of the 28th Annual EMBS International Conference*, pp. 1997-2000, 2006

- J.W. Suh and J.G. Jeon, "Efficient Multiple Memory Control Method for Image Data Processing", *APCC 2003. The 9th Asia-Pacific Conference*, Vol. 2, pp. 830 – 833, Sep. 2003

- S. Kang, H. Hwang, J.W. Suh and Y. Lee, "Reliable and Flexible Video Codec Structure Implemented on a RISC Processor", *Proc. PROMS2000* , pp. 243-246, Oct. 2000.

- J.W. Suh, "A Simplified Subpixel Motion Estimation with Decreased Interpolation and Search", *IEEK Fall Conference*, 1997.

Translation

- "C++ for C programmers" (Hanbit book, Aug. 2000) :
  Korean Language version translated from Original English book "C++: The Core Language" (Satir and Brown, O'Reilly)

PATENTS

- J.W. Suh, S.K. Choi, W.S. Shim, "Method and Apparatus for Accelerating 2-D Graphic Data", *US Patent (US 7,027,060)*, Apr. 11, 2006, *Korea Patent (10-0503085-0000)*

- J.W. Suh, S.U. Kang, "Decoding Method for Reducing Delay Time", *US Patent (US 6,848,013)*, Jan. 25, 2005, *Japan Patent (JP2002027457)*, *China Patent (CN1229989)*

- J.W. Suh, Y.J. Kim, "Apparatus Having Lower Data Transmission Rate and Less Degradation of Image Quality and Method Therefor", *US Patent (US 6,798,915)*, Sep. 28, 2004, *UK Patent (GB2363945)*, *China Patent (CN1144467)*

- J.W. Suh, "Method for Approximating Fast Discrete Cosine Transform", *Korea Patent (10-0677077-0000)*, Dec. 28, 2006

- W.S. Shim, J.W. Suh, "Apparatus and Method For Serial Scaling", *Korea Patent (10-0472464-0000)*, Jul. 14, 2005

- J.W. Suh, K.Y. Ryu, "Motion Estimation Method for Mobile Device", Apr. 23, 2002; *Korea Patent (10-0335434-0000)*

AWARDS

- 3rd place winner for *Paul E. Torgersen Graduate Student Research Excellence Award* March 28, 2007

- Graduate Research & Development Project (GRDP) Grant from Graduate Student Assembly of Virginia Tech, Jan. 2007

- Scholarship, Korea Science and Engineering Foundation Aug. 2003~May 2005

-"*Award for excellent paper announcer*" from IEEK (The Institute of Electronics Engineers of Korea), Feb. 1998